MONTHLY WEATHER REVIEW

VOLUME 81 NUMBER 6

JUNE 1953

CONTENTS

U. S. DEPARTMENT OF COMMERCE • WEATHER BUREAU

PUBLICATIONS OF THE U. S. WEATHER BUREAU

As the national meteorological service for the United States, the Weather Bureau issues several periodicals, serials, and miscellaneous publications on weather, climate, and meteorological science as required to carry out its public service functions. The principal periodicals and serials are described on this page and on the inside of the back cover. A more complete listing of Weather Bureau publications is available upon request to Chief, U. S. Weather Bureau, Washington 25, D. C.

Orders for publications should be addressed to the Superintendent of Documents, Government Printing Office, Washington 25, D. C.

MONTHLY WEATHER REVIEW

First published in 1872, the Monthly Weather Review serves as a medium of publication for technical contributions in the field of meteorology, principally in the branches of synoptic and applied meteorology. In addition each issue contains an article descriptive of the atmospheric circulation during the month over the Northern Hemisphere with particular reference to the effect on weather in the United States. A second article deals with some noteworthy feature of the month's weather. Illustrated. Annual subscription Domestic: $3.50; Foreign, $4.50; 30 cents per copy. Subscription to the *Review* does not include the *Supplements* which have been issued irregularly and are for sale separately.

CLIMATOLOGICAL DATA—NATIONAL SUMMARY

This monthly publication contains climatological data such as pressure, temperature, winds, rainfall, snowfall, severe storms, floods, etc., for the United States as a whole. A short article describing the weather of the month over the United States, tables of the observational data, and a description of flood conditions are supplemented by 15 charts. An annual issue summarizes weather conditions in the United States for the year. More detailed local data are provided in the Climatological Data (by sections) for 45 sections representing each State or a group of States, and Hawaii, Alaska, and the West Indies. Subscription price for either the National Summary or for a Section: $1.50 per year (including annual issue), 15¢ per copy.

(Continued on inside back cover)

The Weather Bureau desires that the *Monthly Weather Review* serve as a medium of publication for original contributions within its field, but the publication of a contribution is not to be construed as official approval of the views expressed.

The issue for each month is published as promptly as monthly data can be assembled for preparation of the review of the weather of the month. In order to maintain the schedule with the Public Printer, no proofs will be sent to authors outside of Washington, D. C.

The printing of this publication has been approved by the Director of the Bureau of the Budget, February 11, 1952.

DEPARTMENT OF COMMERCE
SINCLAIR WEEKS, Secretary

WEATHER BUREAU
F. W. REICHELDERFER, Chief

MONTHLY WEATHER REVIEW

Editor, JAMES E. CASKEY, JR.

Volume 81
Number 6

JUNE 1953

Closed August 15, 1953
Issued September 15, 1953

HORIZONTAL CONVERGENCE AND THE OCCURRENCE OF SUMMER PRECIPITATION AT MIAMI, FLORIDA

STANLEY DAY

Weather Bureau Airport Station, Miami, Fla.

Manuscript received August 4, 1952; revised manuscript received July 8, 1953]

ABSTRACT

The Bellamy nomograph is applied to a triangle over southeastern Florida and adjacent waters to compute the horizontal divergence and convergence in the lower levels for the period June–August 1951. The general diurnal pattern and the extent of the sea-breeze effect are established and graphed, as are the variations in the pattern between wet and dry days. A comparison is made between the results of this study and those obtained from a similar investigation in central Florida. The relationship between the partial and total convergence values and the occurrence of precipitation is examined. The short test period and lack of data prevent any determination of valid forecast rules but a study of the charted data reveals several promising leads meriting further investigation.

INTRODUCTION

Summer showers and thunderstorms of apparent local origin but of severe intensity and with excessive precipitation are a major forecasting problem in Florida, particularly in the southeastern coastal area around Miami. These showers, occurring within a generally uniform unstable mT air mass, are not typically related in time or intensity to the passage of fronts, squall lines, easterly waves of noticeable magnitude, or hurricanes. The purpose of this study is to determine the relationship between horizontal convergence over southeastern Florida as measured by the Bellamy nomograph and the occurrence of summer precipitation.

Examination of previous investigations of the Florida shower problem indicates that theories as to the causes of the development of the large areas of horizontal convergence necessary to widespread thunderstorm activity over Florida cannot be completely reconciled. Riehl [1] ascribes the cause to the presence of a more or less permanent zone of horizontal convergence across the Florida peninsula as a result of a permanent trough of low pressure at some level in the atmosphere. Byers and Rodebush [2] have investigated the Florida thunderstorm as it occurs over the central portion of the State by using the Bellamy nomograph [3]. In their report it is stated that easterly waves, hurricanes, and frontal zones were found to be too rare to account for the almost daily thunderstorm activity in the portion of the State that they were considering. They concluded that the shower activity was set off by a low level mechanism, the conflicting sea breezes of the east and west Florida coasts, meeting over the center of the peninsula. To support this theory graphs of monthly convergence patterns were developed showing the time of maximum occurrence of convergence coinciding with the time of maximum shower occurrence.

The triangle chosen by Byers and Rodebush for the central Florida study, with Jacksonville, Miami, and Tampa at the vertices, was of extensive length with these vertices subject to different maritime exposures. The centroid of this triangle falls somewhere south of Orlando near the location of the Thunderstorm Project of 1946, which provided the basic data. The triangle was chosen deliberately to measure the conflicting sea-breeze effect since it was felt that this was the mechanism that makes possible the daily afternoon thunderstorms over the interior of Florida. The sea breezes establish an organized convergence zone over the peninsula on days when no large scale synoptic disturbance is present, the result of diurnal heating which may be considered as an indirect cause of the inland thunderstorm activity. However, without the converging effect of the double sea breeze over the Florida peninsula, the diurnal heating alone would not produce this activity.

This theory explains the mechanisms in operation over

the central portion of the State but cannot be applied directly to the southeastern coastal area. To understand the shower problem peculiar to Miami and southeastern Florida, and how it differs from the rest of the peninsula, it is necessary to consider the geographical factors involved. Miami is located at the extreme southeastern end of a long, nearly flat peninsula thrust deep into the influence of the trade winds, and into the warm waters of the Gulf Stream. Less than 60 miles to the west are the cooler waters of the Gulf of Mexico. Winds of any direction other than northwest have had at least some recent water trajectory. The prevailing winds over south Florida have easterly or southerly components throughout the summer. As a result the air reaching the peninsula has a water history of extended duration, and is always identifiable as maritime tropical, with slight variation either in dew points in the lower levels or in the lapse rate. Yet with these apparently constant factors, the daily precipitation patterns on the southeastern coast are anything but constant.

Miami and the lower east coast do not experience as many afternoon thunderstorms as the central part of the State, but do have more thunderstorms occurring during the night and morning [4]. Also there are periods of as much as several days in which the lower east coast experiences little or no rain while the precipitation pattern goes on unchanged in the central portions. This would suggest a modification in the cause of the showers as set forth by Byers and Rodebush. It is undoubtedly some combination of the mechanism of the sea breeze and the influence of traveling synoptic features as described by Riehl. Gentry and Moore [5] have investigated the variation of the interaction of the sea breeze and gradient wind flow, the timing of the onset of the sea breeze, and have correlated these factors with the time of shower occurrence in the summer at places within 25 miles of the southeast Florida coast.

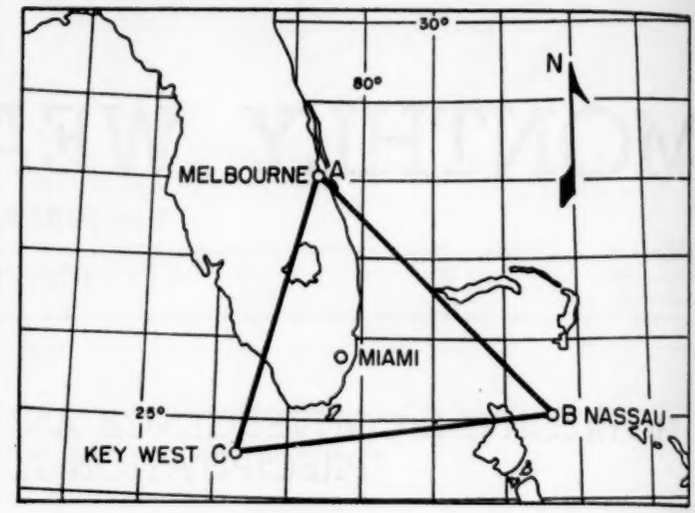

FIGURE 1.—Map of South Florida and adjacent waters showing triangle ABC formed by the pilot balloon stations used in computing convergence at Miami.

30°

KTS	A	B	C
5	-05	-02	+07
10	-10	-04	+15
15	-16	-06	+22
20	-21	-08	+29
25	-26	-10	+36
30	-31	-13	+44
35	-36	-15	+51
40	-42	-17	+59

FIGURE 2.—Sample column of the computed table of divergence (+) and convergence (−) values in units of (3 hr).$^{-1}$ Partial values at stations A, B, and C (see fig. 1) are shown for a 30° wind direction and for the wind speeds (knots) given in the stub.

COMPUTATION OF CONVERGENCE

After the appearance of Bellamy's article [3], a study similar to the one conducted by Byers and Rodebush was set up for the Miami area. Through the fortunate location of pilot balloon stations at Melbourne, Fla. (since replaced by Patrick Air Force Base, Cocoa, Fla.), Nassau, Grand Bahamas, and Key West, Fla., it was possible to set up a nearly equilateral triangle with Miami very near the centroid. (See fig. 1.) Assuming an exact equilateral relationship between the stations facilitated the construction of a table of partial divergence values for each station. Computations were so adjusted that the partial divergence values represent the percentage of volume of air removed or added in a 3-hour period. A sample column of the table is shown in figure 2. Positive values represent divergence, negative values convergence.

Date 7-1-51 Winds Aloft Time 1500 GMT Raob Time 1600 GMT

Winds Aloft:				Computations:				
Hgt.	A	B	C	Hgt.	A	B	C	Total
Sfc.	3406	1315	1508	Sfc.	+02	-20	-03	-21
1000	3508	1415	1506	1000	+02	-19	-02	-19
2000	3510	1414	1606	2000	+02	-18	-04	-20
3000	3513	1414	1605	3000	+02	-18	-03	-19
4000	3311	1514	1803	4000	+08	-15	-04	-11
5000	3310	1513	1803	5000	+07	-13	-04	-10

Precipitation:

Miami WBAS 6 hr 1830 GMT to 0030 GMT .15 12 hr 0030 GMT to 0630 GMT 0

Miami WBO " " .59 " " 0

FIGURE 3.—Sample worksheet on which pibal data and convergence computations for stations A, B, and C were recorded every 6 hours.

Beginning at 0300 GMT, June 1, 1951, and at each 6-hourly pibal observation thereafter, a record was kept of the partial divergence values for each station of the triangle, with the algebraic summations assumed to be the net effect upon the centroid, Miami. Due to the inconsistencies of the pibal observations in reaching

heights above 5,000 feet, this study was limited to data compiled below that height. Also tabulated were the precipitation records from both the Miami Weather Bureau Airport Station and the Miami City Office. This record was concluded with the 2100 GMT observation, August 31, 1951. A sample data sheet is shown in figure 3.

AVERAGE DIURNAL VARIATION OF CONVERGENCE

The daily convergence patterns for each month and the average convergence for the entire period were computed and graphed as shown in figure 4. These curves show a diurnal fluctuation of convergence that varies from month to month in intensity, yet they are fairly consistent in general pattern and average out over a longer period into a symmetrical curve. The variation of daily oscillations can be related to the daylight and darkness periods, and thus may reflect the land-sea relationship. The 0300 GMT readings indicate strong divergence, while this is completely reversed by the daytime circulation pattern at 1500 GMT. At 2100 GMT the figures average out to produce a neutral effect, all levels falling on or near the zero line. In the July and August charts the symmetry of the curves becomes more pronounced with the convergence peak falling decisively at 1500 GMT, and the levels arranging themselves in order, with a minimum of convergence and even divergence appearing around 4,000 to 5,000 feet, representing a "spill-over" of the rising column of air. In August this is especially well marked.

The 3-month averages produce a symmetrical pattern with the levels arranging themselves in almost exact order at the 0300 GMT and 1500 GMT observations, and passing through a "node" or neutral stage at both the 0900 GMT and 2100 GMT observations. The monthly curves become more orderly in their behavior as summer advances, approaching the average curve. This can be best explained by considering that in June the air mass distribution of the lower peninsula is not completely maritime

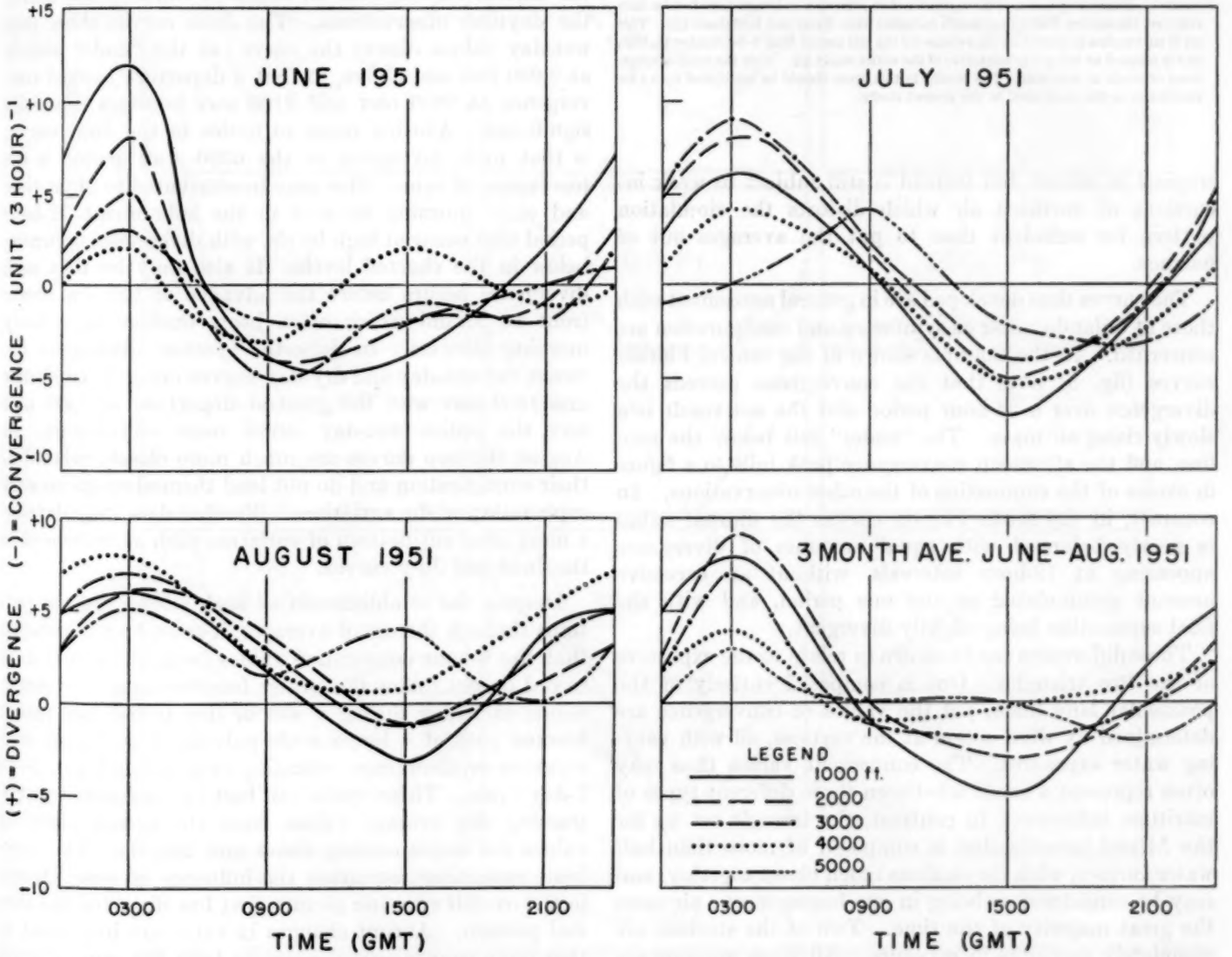

FIGURE 4.—The average diurnal variation in divergence and convergence at Miami, Fla., for levels 1,000 feet through 5,000 feet for June, July, and August 1951, and for the 3-month season.

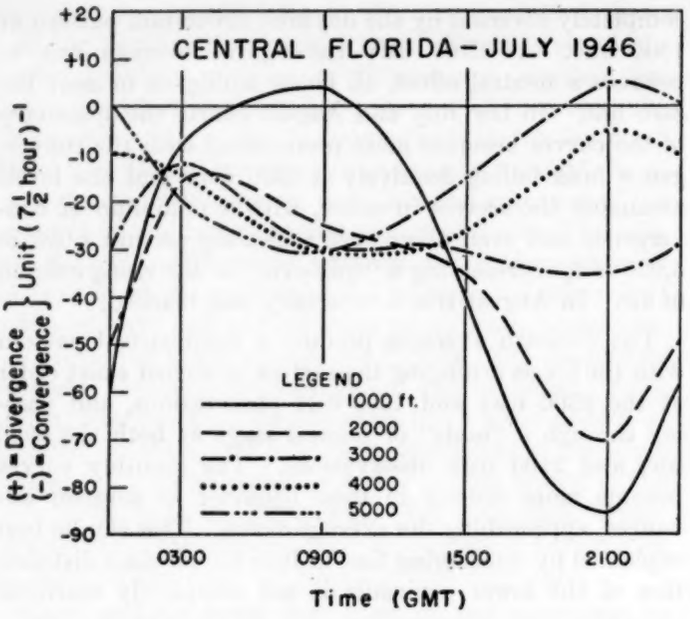

FIGURE 5.—Diurnal variation of divergence and convergence in lowest 5,000 feet for July 1946 over the central Florida peninsula (adapted from Byers and Rodebush [2]). This set of curves closely resembles the average for the test period May 1–September 15, 1946, and is selected as being representative of the entire study [2]. Note the exact arrangement of levels at 2100 GMT. The results in this figure should be multiplied by 0.4 for conversion to the units used in the present study.

tropical in nature, but instead is still subject to weak incursions of northern air which distorts the circulation pattern for sufficient time to put the averages out of balance.

The curves thus developed are in general agreement with those at Orlando so far as symmetry and configuration are concerned. In the example shown of the central Florida curves (fig. 5) note that the convergence exceeds the divergence over a 24-hour period and the net result is a slowly rising air mass. The "nodes" fall below the zero line, and the afternoon convergence peak falls to a figure in excess of the summation of the other observations. In contrast, in the south Florida curves the diurnal swing is nearly balanced with equal amounts of divergence appearing at 12-hour intervals, without an excessive amount accumulated at any one period, and with the final summation being slightly divergent.

These differences can be shown to relate to the exposures of the two triangles. One is composed entirely of the peninsular land mass, yet the values of convergence are determined by wind action at the vertices, all with varying water exposures. The convergent values thus may often represent a conflict between three different types of maritime influence. In contrast, the triangle set up for the Miami investigation is composed of more than half water surface, with the stations much closer together, and may be considered as being in one homogeneous air mass the great majority of the time. Two of the stations are completely maritime in exposure. All three stations are on the same side of the peninsula in relation to the large scale easterly flow, and the variations in the types of sea breeze at the separate vertices can be considered to be minimized.

CONVERGENCE AND PRECIPITATION RELATIONS

In order to determine the changes in the convergence pattern that relate to changes in the precipitation pattern, the data were broken down into two sets, corresponding to rain and no-rain days, and replotted. Wet days were considered to be those on which a trace or more of rain was recorded at either the Miami Airport Station or City Office within 12 hours following the time of the wind observations. A dry day was one on which no rain was measured at either station during the same period.

In figure 6 the wet-day and dry-day convergence curves for the separate months and the 3-month average are shown for the lower 3,000 feet. Note that the wet-day curves in most instances appear to be exaggerations of the normal curves, with an excess of convergence during the daytime observations. The June curves show that wet-day values distort the curve at the "node" periods at 2,000 feet and above, so that a departure toward convergence at 0900 GMT and 2100 GMT becomes especially significant. Another point to notice in the June curves is that more divergence at the 0300 GMT period is the forerunner of rain. This may be attributed to night-time and early morning showers in the subsequent 12-hour period that occur at high levels, with divergence occurring below in the charted levels. It also may be that such divergence occurs before the advance of the sea breeze front at Miami which often bears onshore light early morning showers. In July the greatest differences between the wet-day and dry-day curves occur at 0300 GMT and 1500 GMT with the greatest departure at 1500 GMT and the entire wet-day curve more convergent. In August the two curves are much more closely related in their configuration and do not lend themselves to an easy explanation of the variations. Further data may develop a more clear cut pattern of variation such as evidenced in the June and July curves.

Despite the establishment of such strong diurnal patterns through the use of averages, it must be remembered that the 6-hour consecutive values from the actual data record do not follow the swings from strong plus to strong minus each day during a wet or dry period but rather become part of a larger scale pattern of sustained convergence or divergence extending over as much as a 5- to 7-day cycle. These cycles can best be measured by subtracting the average values from the actual observed values for corresponding times and heights. The algebraic remainder represents the influence of some change in the overall synoptic picture that has distorted the normal pattern. Abrupt changes in value are important in that large convergence departures from the general trend of the observed curve were noted to precede rain of considerable intensity or an extended period of shower activ-

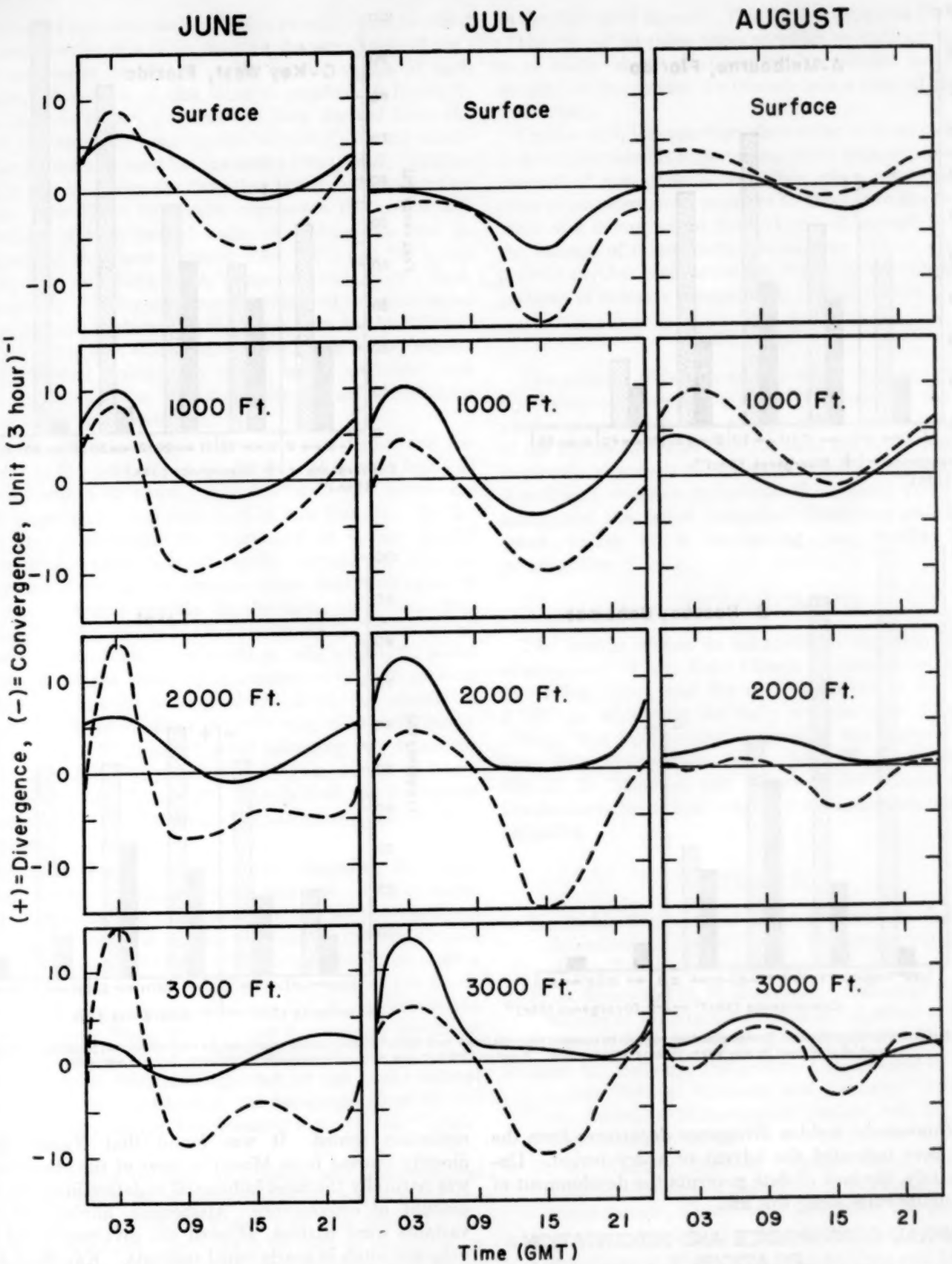

FIGURE 6.—The average diurnal variation of divergence and convergence for wet days (dashed line) and dry days (solid line) at Miami, Fla., by altitude and by months. Wet day means trace or more of rain at either WBO or WBAS, Miami; dry day means no rain at either measuring station.

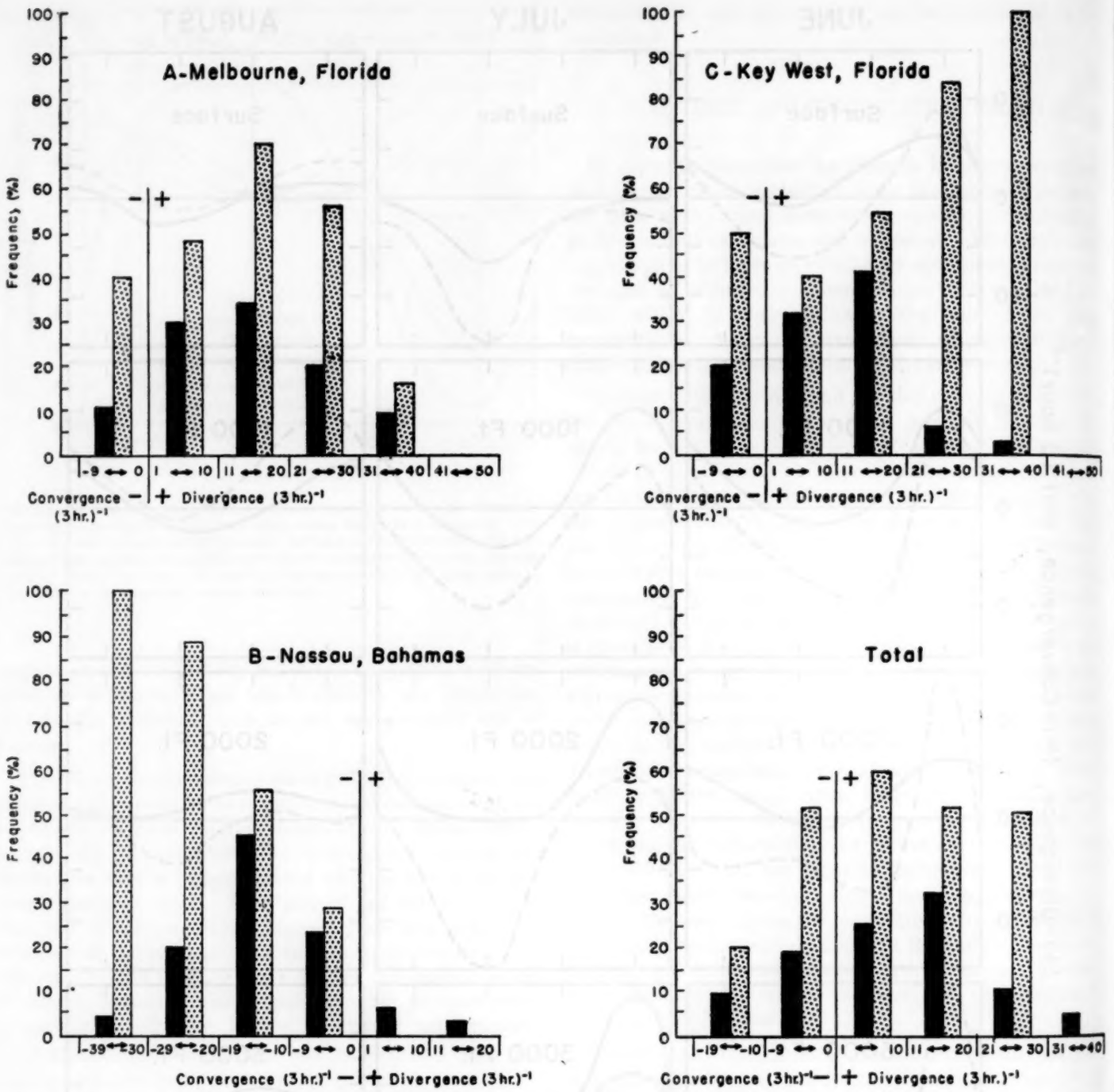

FIGURE. 7—Percentage of occurrence of divergence and convergence by classes of ten units (black bars) for each station (partial values) and for total values; and percentage of occurrence of each class followed by rain within 12 hours (stippled bars). Based on 1,000-foot data, 0300 GMT observation, for the entire 3-month test period.

ity. Conversely, sudden divergence departures from the curve have indicated the advent of a dry period. Unfortunately, the lack of data prevents the development of any definite rules along this line.

PARTIAL CONVERGENCE AND PRECIPITATION RELATIONS

The next step was to determine to what extent the partial values of each of the vertices influence the total, and if possible how the influence could be related to the precipitation record. It was found that Nassau, being directly upwind from Miami in most of the observations, was naturally the most influential in determining the total amount of convergence. Melbourne, having the most variable wind pattern, affected the divergence and convergence totals in nearly equal amounts. Key West, being farther removed from the wind pattern that affects the east coast, contributed the least to the variations of convergence, but was the most responsible for the occurrence of large divergence readings.

To relate this information to the precipitation required the construction of a table showing the percentage of wet-day occurrence as related to the partial values at each station. A section of this table is graphed in figure 7. The example shown contains the data derived from the 1,000-foot values of convergence at the 0300 GMT observation period averaged for the entire test period. Similar graphs can be drawn for the other levels and observation times. The black bar-graph represents the percentage frequency of each partial value of convergence and divergence at the three vertices, "A", "B", and "C", corresponding to Melbourne, Nassau, and Key West, respectively. The percentage frequency of the summation of the partials is shown by the black bars on the "Total" graph. Note that this portion of the graph is very similar to the normal distribution curve, and if sufficient data were introduced into the study the normal distribution would likely be approached.

The stippled bar-graph represents the percentage frequency of the partial and total values that were followed by rain within 12 hours. The "B" and "C" curves are most significant when examined in this respect. On the "B" graph, although the frequency of strong partial convergence values falls off rapidly toward the left, the frequency of strong convergence values that were followed by rain increases rapidly in the same direction. For example, while values -10 to -19 $(3\text{ hr.})^{-1}$ occur 45 percent of the time, they result in rain within 12 hours 56 percent of the time. The occurrence of -20 to -29 $(3\text{ hr.})^{-1}$ is but 20 percent of the total, but almost 90 percent of these readings precede rain within 12 hours, and -30 to -39 $(3\text{ hr.}),^{-1}$ while occurring but 4 percent of the time are always followed by rain within 12 hours for a reading of 100 percent. The data on the divergence side of the "B" graph are very limited but suggest a no-rain situation.

However, the "C" graph shows increasing likelihood of rain as the divergence values increase. The relationship of this rather unexpected factor to the resultant rain is best found in an examination of the wind shifts around an easterly wave. With such a wave near or over Miami, Nassau (or "B") being to the east of the wave, has a southeast or convergent wind with relation to the triangle. Key West, or "C", has a divergent northeast wind west of the trough. Melbourne, or "A", shows no variation other than that expected by use of the normal curve. The two portions of the bar-graph show similar tendencies throughout, and the same is true of the "Total" graphs.

Similar graphs for the other levels and observational periods show that the relationship of the partials and the total to the precipitation varies with the time of day. The totals are most important in relation to precipitation in the 1500 GMT data, while the partials are not clearly related. At 0900 GMT and 2100 GMT little can be derived from either the partials or the total as they relate to the likelihood of rain. This further supports the theory of the "node" at those times at which no indicative differences can be detected at any level or station and the air circulation throughout the triangle is in a state of confused transition.

From a complete set of graphs similar to those in figure 7 it should be possible to formulate some type of probability forecast of rain occurrence. This, when combined with other parameters, may prove to be the key to the development of a measurement method critical enough to detect the passage of minor disturbances over Miami, and thus provide another tool for the job of solving the troublesome problem of summer precipitation at that station.

CONCLUSION

The original objective of this study was to formulate some clear-cut forecasting rules by correlating the divergence values with the precipitation record. Analysis of the results indicates that the data are much too sparse to permit any such definition of rules. However, there is sufficient evidence to indicate the general value of the study, and the use of computed divergence and convergence values as a forecasting tool merits further investigation.

ACKNOWLEDGMENTS

The author wishes to acknowledge the help and encouragement of Mr. Robe Carson in developing the data to its final form, and the other members of the Miami FAWS in tabulating the daily records. Dr. Charles S. Gilman was instrumental in guiding the analysis of the data into the proper form. Mr. W. L. Thompson, Mr. P. D. Thomas, and others of the Miami Airport Station have been most helpful in the assistance they have extended.

REFERENCES

1. H. Riehl, "Subtropical Flow Patterns in Summer," *Miscellaneous Report* No. 22, Department of Meteorology, University of Chicago, 1947, 64 pp.
2. H. R. Byers and H. R. Rodebush, "Causes of Thunderstorms of the Florida Peninsula," *Journal of Meteorology*, vol. 5, No. 6, Dec. 1948, pp. 275–280.
3. John C. Bellamy, "Objective Calculations of Divergence, Vertical Vorticity, and Velocity," *Bulletin of the American Meteorological Society*, vol. 30, No. 2, Feb. 1949, pp. 45–49.
4. U. S. Weather Bureau, "Thunderstorm Rainfall," *Hydrometeorological Report* No. 5, Waterways Experiment Station, Vicksburg, Miss., 1945, 330 pp.
5. R. C. Gentry and Paul L. Moore, Relation of Sea Breeze and General Wind Interaction to Time and Location of Air Mass Showers, U. S. Weather Bureau Office, Miami, Fla. (Unpublished manuscript.)

FREQUENCY VARIATION OF SNOW DEPTHS IN THE MISSOURI AND UPPER MISSISSIPPI BASINS

VANCE A. MYERS

Hydrometeorological Section, U. S. Weather Bureau, Washington, D. C.

[Manuscript received May 13, 1953]

The accumulated depth of snow is a weather element not usually summarized in Weather Bureau climatological publications. Recently certain snow-depth frequencies were compiled for a number of first-order Weather Bureau stations in or near the drainage area above St. Louis, Mo., in connection with a study of the flood potential at St. Louis. The snow-depth frequencies are presented in table 1, for the benefit of others who may have use for these data.

Daily accumulated depths of snow on the ground (in inches) were taken from W. B. Form 1001, "Original Monthly Record of Observations," and were plotted against day of the year. Smooth curves were drawn, one enveloping all the points, one enveloping 95 percent, and another enveloping 90 percent. To construct the latter two curves, 10-day periods were considered as units. Except for minor adjustments for smoothing, the number of dots within a 10-day period (February 1–10, 11–20, etc.) lying above the 90 percent curve (exceeded 1 year in 10) equalled the number of years of record, with half that many dots above the 95 percent curve (exceeded 1 year in 20). Depths were read from the curves at 10-day intervals, and are presented in table 1. Traces were not considered and were plotted as zeros. Therefore, the zeros in the table should be interpreted as less than 0.1 inch. Since there is considerable variation from station to station when these data are plotted on maps, and since such maps are not readily subject to a logical analysis, this form of presentation was discarded.

Appreciation is expressed to the National Weather Records Center which furnished a large number of photostats and to Margaret E. Linehan, A. E. Brown, A. L. Criss, J. L. Keister, J. T. Lindgren, and H. H. Vinnedge of the Hydrometeorological Section staff who took part in processing the data.

TABLE 1.—*Depths of snow on ground (inches) exceeded 10 percent and 5 percent of the years on certain dates, and maximum snow-depth values for those dates*

Station	Years	February 10			February 20			February 28			March 10			March 20			March 31			April 10			April 20			April 30		
		10%	5%	Max.	10%	5%	Max.	10%	5%	Max.	10%	5%	Max.	10%	5%	Max.	10%	5%	Max.	10%	5%	Max.	10%	5%	Max.	10%	5%	Max.
Cairo, Ill.	1893–1948	0.5	1.6	9.7	0	0.7	8.9	0	0	7.7	0	0	5.7	0	0	3.2	0	0	1.0	0	0	0.4	0	0	0.2	0	0	0
Charles City, Iowa	1905–48	11.5	16.6	22.4	9.0	17.0	26.9	7.0	12.5	29.3	4.5	7.0	23.5	1.9	4.2	17.0	0	1.6	11.0	0	0	6.1	0	0	2.5	0	0	0
Columbia, Mo.	1893–1948	3.0	5.6	10.8	3.0	6.2	12.5	1.4	3.4	13.0	0	1.4	12.9	0	0	11.9	0	0	9.4	0	0	4.4	0	0	0	0	0	0
Davenport, Iowa	1893–1948	6.8	8.8	14.4	3.7	6.3	13.9	2.5	4.1	13.3	1.8	3.1	12.5	.5	1.8	11.6	0	.4	10.2	0	0	8.4	0	0	5.0	0	0	0
Des Moines, Iowa	1893–1948	6.4	9.0	21.5	3.9	7.9	20.9	2.9	6.9	19.8	2.0	5.1	17.4	.8	2.7	14.4	0	.8	11.0	0	0	9.4	0	0	8.4	0	0	6.7
Devils Lake, N. Dak.	1905–46	11.7	14.3	30.0	11.8	14.7	27.8	10.7	14.0	25.5	7.3	11.0	21.5	4.2	6.9	17.8	1.8	3.5	14.0	.2	1.2	10.8	0	0	7.5	0	0	4.6
Dodge City, Kans.	1893–1948	0.9	2.4	6.8	1.1	3.4	13.7	1.2	4.4	15.2	0	4.6	15.5	0	.2	15.0	0	0	13.5	0	0	11.5	0	0	8.3	0	0	0
Dubuque, Iowa	1893–1948	8.6	12.9	26.8	6.4	11.6	21.7	4.5	7.1	18.4	3.0	4.6	15.0	1.7	3.1	12.6	0	1.3	10.1	0	0	7.4	0	0	4.4	0	0	1.0
Ellendale, N. Dak.	1918–33	9.4	10.6	15.0	8.8	11.2	16.4	5.2	11.2	14.9	1.9	5.1	12.2	0.9	2.0	9.7	.4	1.2	6.8	0	.7	4.2	0	0	2.2	0	0	1.1
Grand Forks, N. Dak.	1914–48	16.9	18.1	22.9	17.2	18.5	23.4	15.7	19.0	23.9	12.4	18.5	24.1	7.8	12.3	17.2	3.3	5.0	11.3	.1	1.5	7.3	0	0	4.7	0	0	3.2
Hannibal, Mo.	1893–1933	4.0	7.7	15.0	1.0	7.5	16.8	.8	2.0	17.0	.7	2.4	16.2	0	.8	14.6	0	.1	12.2	0	0	6.5	0	0	1.5	0	0	0
Iola, Kans.	1906–36	.4	1.2	10.7	0	.9	11.8	.1	1.7	12.0	0	2.0	11.7	0	0	10.7	0	0	5.2	0	0	0	0	0	0	0	0	0
Kansas City, Mo.	1893–1943	2.8	4.8	14.9	1.4	4.2	15.6	.7	2.4	16.4	.2	2.6	18.0	0	.8	19.8	0	.1	16.5	0	0	7.0	0	0	4.2	0	0	2.2
Keokuk, Iowa	1893–1941	4.7	8.7	12.8	3.0	8.7	13.0	1.3	3.2	13.0	0	1.5	12.9	0	.6	12.7	0	.1	12.3	0	0	3.5	0	0	.4	0	0	0
LaCrosse, Wis.	1893–1948	12.8	16.9	28.5	11.0	14.3	28.3	9.1	11.7	27.8	5.3	8.3	16.1	2.7	5.1	14.0	0	2.4	12.7	0	0	1.1	0	0	8.3	0	0	2.0
Lincoln, Nebr.	1897–1948	5.0	7.3	16.9	3.3	7.4	17.3	2.7	7.3	17.2	2.5	6.8	16.7	.5	2.2	11.8	0	.2	8.4	0	0	6.4	0	0	4.2	0	0	0
Madison, Wis.	1905–48	13.3	16.7	21.9	9.5	16.2	22.2	7.7	10.8	20.2	5.6	7.5	17.3	3.2	5.8	15.0	.7	3.2	12.9	0	.8	11.4	0	0	8.7	0	0	3.8
Minneapolis, Minn.	1899–1948	12.9	14.2	21.8	12.0	13.8	29.9	9.8	13.2	32.2	5.6	10.0	32.4	2.7	6.9	28.0	.8	2.7	13.2	0	.4	11.2	0	0	9.7	0	0	6.7
Moorhead, Minn.	1893–1938	15.3	17.7	26.1	15.0	17.6	26.9	12.4	17.5	27.5	8.8	12.3	27.8	7.0	9.7	26.0	2.2	5.4	17.8	.4	1.5	12.3	0	.3	6.9	0	0	3.5
North Platte, Nebr.	1893–1948	2.7	3.5	13.2	1.6	2.9	14.1	1.6	3.1	14.4	1.3	3.3	14.2	.7	2.8	12.9	0	1.8	7.5	0	0	5.6	0	0	4.2	0	0	3.1
Omaha, Nebr.	1893–1943	5.3	8.3	19.6	4.4	7.7	19.9	4.2	6.2	19.9	3.1	5.8	19.5	1.6	2.9	14.8	0	.5	8.6	0	0	4.9	0	0	2.4	0	0	0
Peoria, Ill.	1905–48	3.3	5.9	11.2	1.5	4.0	11.1	.9	2.3	10.8	.4	2.0	10.4	0	.6	9.7	0	.1	8.4	0	0	4.5	0	0	1.3	0	0	0
Pierre, S. Dak.	1893–1933	4.6	6.2	12.0	3.1	4.3	11.9	2.9	6.0	11.7	3.9	6.7	11.4	2.9	5.4	10.8	.9	2.1	9.9	0	.1	8.4	0	0	6.0	0	0	0
Rapid City, S. Dak.	1893–1948	2.8	4.9	12.2	2.6	4.1	12.4	2.6	3.5	12.8	2.9	4.9	13.5	2.9	5.2	14.5	1.7	4.3	17.0	0	2.2	17.7	0	.2	10.0	0	0	4.0
St. Louis, Mo.	1893–1947	1.8	3.4	15.3	1.6	3.3	15.6	.7	2.1	15.3	0	1.0	12.8	0	.3	10.1	0	0	7.4	0	0	5.2	0	0	2.6	0	0	0
St. Paul, Minn.	1893–1933	14.0	16.5	34.0	13.3	15.4	34.7	12.3	14.0	32.9	8.3	12.1	29.4	2.3	7.2	23.5	.7	2.8	17.4	0	.9	13.9	0	0	11.0	0	0	7.4
Sioux City, Iowa	1893–1948	6.7	10.0	26.0	4.0	6.3	26.3	3.0	4.7	26.2	1.9	3.5	25.9	.8	2.3	25.3	.1	.8	24.1	0	0	20.0	0	0	4.8	0	0	3.0
Springfield, Ill.	1893–1948	2.9	5.4	13.2	1.7	5.2	13.7	.8	2.5	13.7	.1	1.3	13.4	0	.6	11.5	0	0	6.4	0	0	4.1	0	0	2.2	0	0	.2
Springfield, Mo.	1893–1948	1.8	3.8	15.1	1.7	3.7	20.0	.5	2.2	18.9	.1	1.2	15.0	0	.1	10.1	0	0	4.5	0	0	2.3	0	0	.7	0	0	0
St. Joseph, Mo.	1910–43	2.6	5.4	10.7	2.6	5.7	11.3	3.1	5.9	11.5	.1	1.7	11.4	0	.1	10.9	0	0	9.8	0	0	8.1	0	0	0	0	0	0
Topeka, Kans.	1899–1943	3.7	5.1	17.8	1.2	4.8	18.5	1.2	4.9	18.6	.9	2.7	18.2	0	.8	17.2	0	0	14.7	0	0	3.4	0	0	1.4	0	0	.2
Valentine, Nebr.	1893–94 1901–48	3.3	5.6	29.0	3.3	6.9	29.2	3.5	7.9	29.1	3.8	7.8	28.8	3.6	6.6	28.3	.8	2.8	27.7	0	.6	26.9	0	0	17.0	0	0	7.1
Wausau, Wis.	1916–33	20.8	21.7	25.0	20.7	22.6	26.0	20.4	24.0	26.5	16.5	21.8	24.6	6 7	9.7	18.0	3.6	5.3	13.7	2.0	3.8	11.0	0	0	6.0	0	0	0
Wichita, Kans.	1893–1948	.6	2.0	7.4	.3	1.7	8.1	.3	1.7	8.4	.4	1.9	8.5	0	.5	8.3	0	0	7.4	0	0	2.8	0	0	.8	0	0	0
Williston, N. Dak.	1894–1948	10.3	15.3	18.8	9.0	15.1	20.4	7.4	10.4	22.6	6.2	9.7	28.0	6.2	9.8	28.0	3.0	6.1	25.4	0	2.2	21.0	0	0	17.1	0	0	13.6
Yankton, S. Dak.	1893–1933	7.4	11.5	21.8	4.4	7.1	21.1	2.9	5.5	20.0	3.0	5.3	16.2	1.9	5.2	13.4	0	1.2	11.8	0	0	10.0	0	0	7.2	0	0	4.0

THE WEATHER AND CIRCULATION OF JUNE 1953[1]—

The Second Successive June with Record-Breaking Drought and Heat

JAY S. WINSTON

Extended Forecast Section, U. S. Weather Bureau, Washington, D. C.

DROUGHT AND HEAT

Extremely dry weather prevailed over the lower Mississippi Valley, Southern Great Plains, and Southwest during June 1953. Much of this vast area received less than 25 percent of normal rainfall and nearly all of it less than 50 percent (Chart III–B). The dry spell over the South, which began in the last third of May, resulted in extensive deterioration of crops and pastures and desiccation of ponds and streams.

The most severe drought conditions existed over western Texas and in the Rio Grande Valley where, except for brief periods of temporary relief, precipitation has been deficient for nearly 3 years. For example, records at Del Rio and Big Spring, Tex., show that these stations have received respectively only 38 percent and 50 percent of their normal precipitation during the past 33 months. The bed of the Rio Grande dried up at Laredo, Tex., this month for the first time in recorded history. Amarillo, Tex., experienced its driest June on record with rainfall totalling a meager 0.01 inch. Newspaper reports have called this the worst drought in Texas history and have described the appearance of a new "dust bowl" where crop lands have been turned into sand dunes; most ponds, lakes, and streams are bone dry; and crops are stunted or dead.

Other States seriously affected by drought were Oklahoma, Arkansas, Tennessee, and Mississippi, where widespread crop damage and water shortages were reported. Record or near record low rainfall amounts were observed at several stations in these States. One of these was Memphis, Tenn., with 0.04 inch, the lowest amount on record for June.

A prolonged and extreme heat wave accompanied and contributed to the drought, except in southern California and Arizona where temperatures averaged below or near normal (Chart I–B). Maximum temperatures in the 90's or higher occurred nearly every day of the month over most of the drought area. In the Rio Grande Valley there were very few days when afternoon temperatures did not reach 100°. At Laredo, Tex., the maxima varied between 98° and 107° with only 4 days below 100°. Twenty-one consecutive days with maximum temperatures of 100° or more at Abilene, Tex., set a new record for June. At many stations in Texas, Oklahoma, Kansas, New Mexico, Louisiana, Arkansas, and Tennessee monthly mean temperatures were the highest on record for June. At Memphis, Tenn., and Lake Charles, La., June 1953 was not only the warmest June on record but also the hottest month ever observed.

Many of the new heat records established this June just barely exceeded previous records set only last June [1]; while in many places, especially in the central Plains

[1] See charts I–XV following p. 178 for analyzed climatological data for the month.

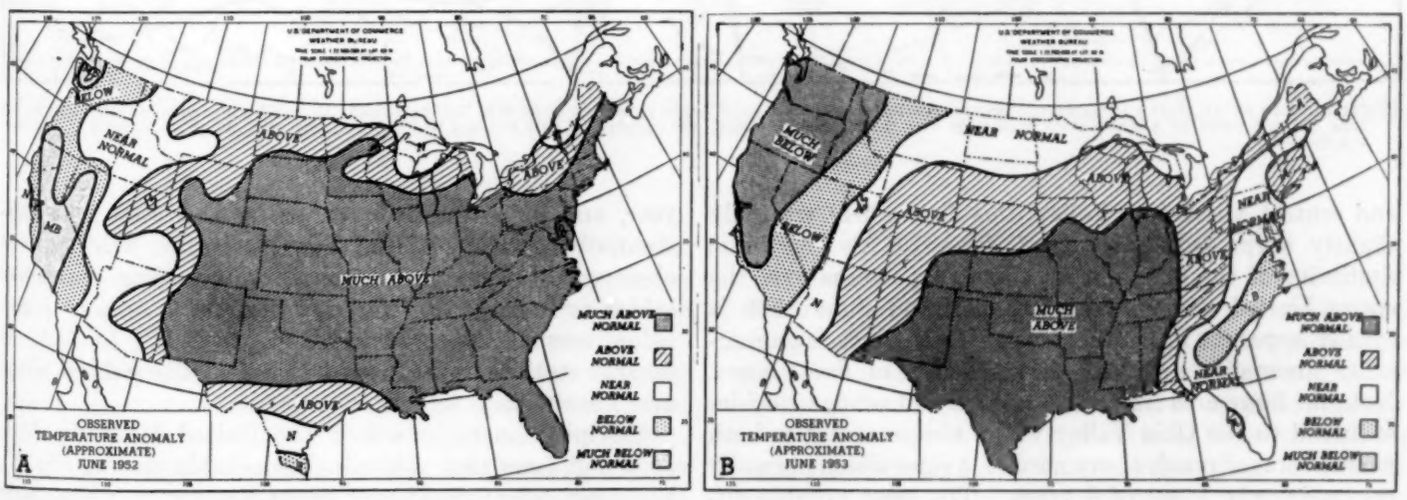

FIGURE 1.—Monthly mean surface temperature anomalies for (A) June 1952 and (B) June 1953. The classes above, below, and near normal occur on the average one-fourth of the time, while much above and much below each normally occur one-eighth of the time. Note the marked similarity in overall pattern, especially the coincidence of much above normal temperatures over a broad area in the central part of the United States.

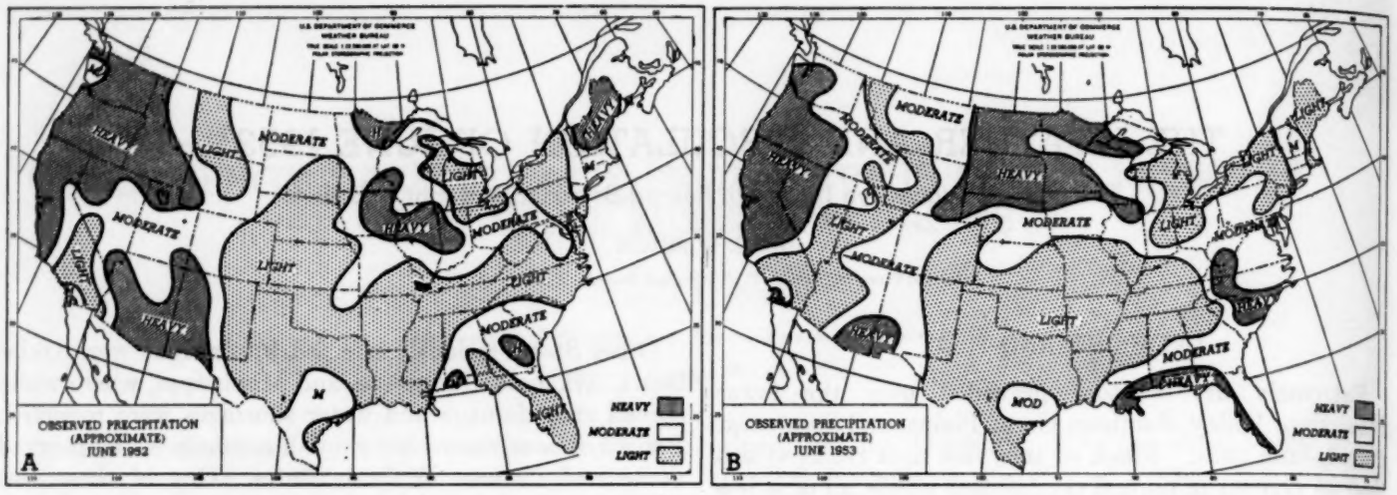

FIGURE 2.— Anomalies of total monthly precipitation for (A) June 1952 and (B) June 1953. The classes light, moderate, and heavy occur on the average one-third of the time. Note general coincidence of like precipitation classes, especially large area of light rainfall over South Central United States in both years.

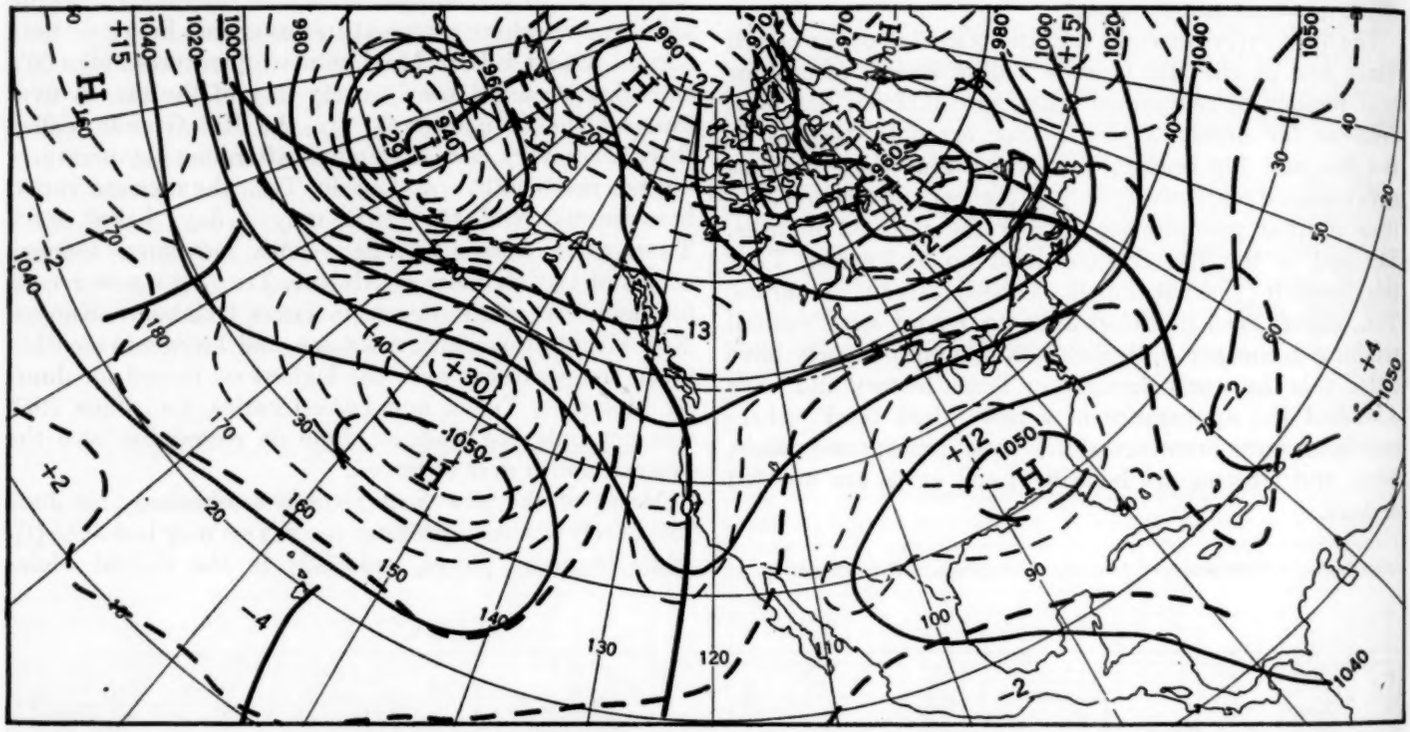

FIGURE 3.— Mean 700-mb. chart with height contours and departures from normal (both labeled in tens of feet) for May 31–June 29, 1952. Circulation over much of United States last June was dominated by a strong subtropical ridge over the Mississippi Valley, accompanied by heat and dry weather over large portions of the country. (See figs. 1-A and 2-A.)

and central Mississippi Valley, this June's heat was only slightly surpassed by that of June 1952. The basic similarity of the temperature anomaly patterns over the entire United States for June 1952 and June 1953 is readily apparent in figure 1, where mean surface temperature anomalies are analyzed in terms of five classes. Note the large area from the southern and central Rockies eastward to the Ohio Valley where temperatures in both years averaged much above normal, a class which normally occurs in only 1 out of 8 years. The most notable differences between the two patterns were along the east coast, where this June was considerably cooler than last year, and in southern Texas, where this June was substantially hotter. In the Far West cool weather was observed in both years, but this June was somewhat colder as indicated by the more extensive area of much below normal temperatures in figure 1-B. In fact, at several stations in this area this was the coldest June ever observed.

Precipitation regimes over the United States in June 1952 and June 1953 were also remarkably similar (fig. 2). Light rainfall occurred over a broad region from Colorado and New Mexico eastward to the Appalachians in both months, generally over the same region where much-

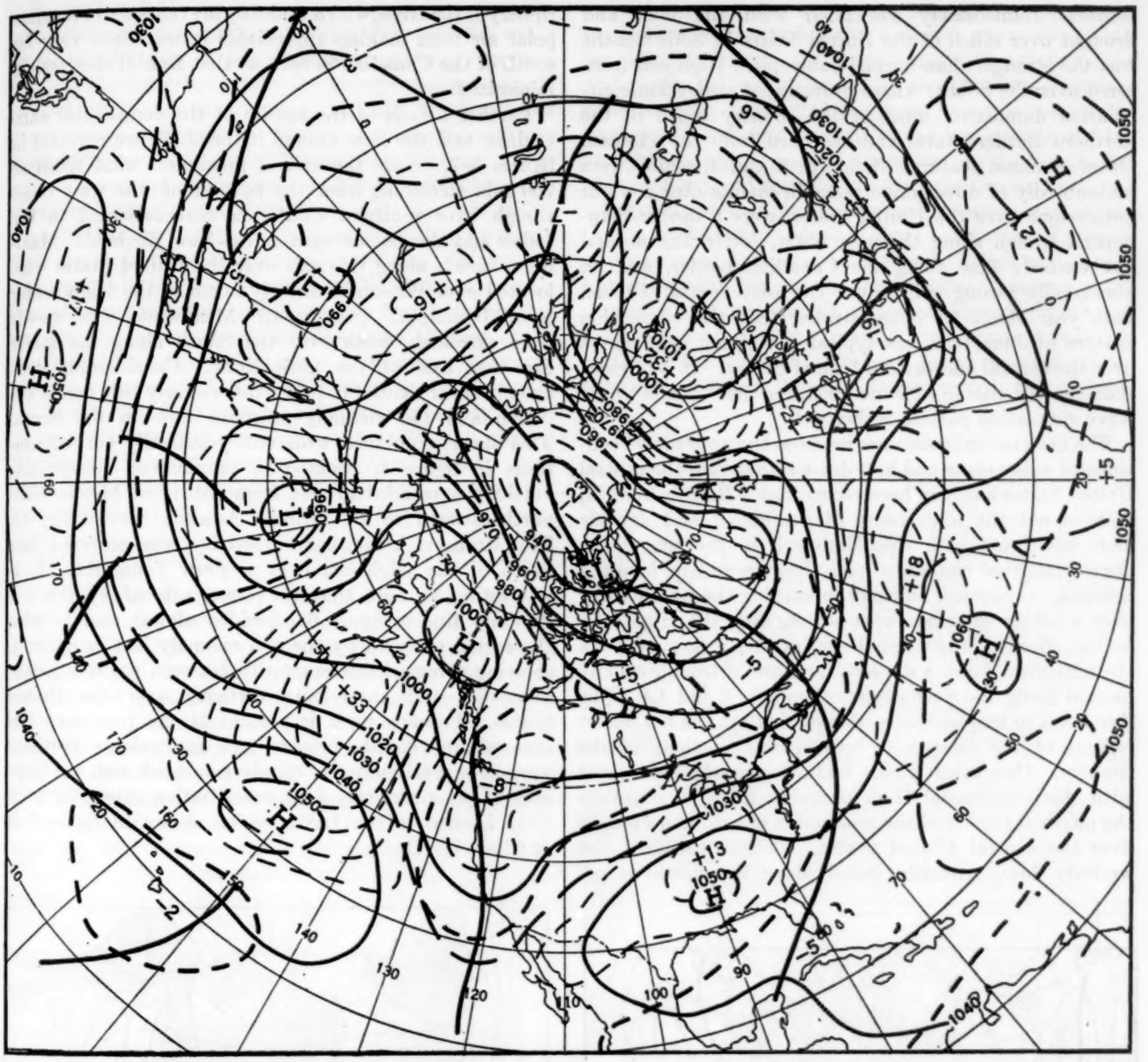

FIGURE 4.—Mean 700-mb. chart with height contours and departures from normal (both labeled in tens of feet) for May 30–June 28, 1953. Note remarkable similarity in basic wave pattern at middle latitudes from western Pacific to central Atlantic between this June and last June. (See fig. 3.) Once again a well-developed continental anticyclone dominated the circulation over the United States with accompanying heat wave and drought. (See figs. 1-B and 2-B.)

above-normal temperatures were observed (fig. 1). Another sizeable area where precipitation was similar in both months was in the Far West where heavy amounts occurred. Other coincidences between precipitation regimes occurred, although on a smaller scale, such as heavy precipitation in southern Arizona and New Mexico, and light in the Lower Lakes, New York, and New Jersey. The major differences were over the northern Plains, the Carolinas, and Florida where this June's precipitation was considerably greater, and over New England where it was considerably lighter than last June's.

RELATED CIRCULATION FEATURES

Since June 1952 and June 1953 showed such good correspondence in both precipitation and temperature regimes over large areas of the United States it is not surprising that the mid-tropospheric circulation patterns were very similar in both months over most portions of North America and adjoining oceans (figs. 3 and 4). The entire wave train from the western Pacific to the Central Atlantic was virtually identical in trough and ridge positions and in locations of major height anomaly

centers. Immediately associated with the heat and drought over much of the United States in both months was the stronger-than-normal subtropical High cell (centered over the South) whose pronounced anticyclonic circulation dominated most of the country south of the northern Border States and eastward from the Plateau. Other common features of figures 3 and 4, which were undoubtedly of direct importance in maintaining a warm anticyclone over the United States, were a deeper-than-normal trough along the west coast, faster-than-normal flat westerly flow along the Canadian border, and an abnormally strong ridge over the east central Pacific. Last year Klein [1] demonstrated that the circulation pattern of June 1952 was typical of summer heat waves over the central and eastern United States. It is obvious that the circulation of June 1953 fits this "model" heat wave circulation pattern rather well.

The association in summer between the upper-level continental anticyclone and hot, dry weather over the central United States has long been recognized. Reed in 1937 [2] pointed out the importance of subsidence and dry air aloft associated with this High cell in preventing the development of cloudiness and showers and in favoring drought. Also of significance in keeping the weather dry over a rather extensive area surrounding the High may be the stronger-than-normal southwesterly flow between the anticyclone and a deeper-than-normal trough usually located along the west coast. (See figs. 3 and 4.) This flow leads to frequent advection of air from the hot desert regions of the Southwest into central portions of the country. One other major feature generally associated with this continental High probably helps to complete the physical picture of the production of heat and drought over the central United States. This is the fast, flat westerly flow, generally found along the northern periphery of the High, which typically prevents cool Canadian polar air from making appreciable penetrations very far south of the Canadian border, so that frontal showers are minimized.

Further details of the nature of the continental anticyclone and the flow around it this June are revealed in figures 5–7. Note the axis of maximum wind speed at 700 mb. stretching from the bottom of the west coast trough over southern California northeastward to the Lakes and thence eastward across New England. Maximum speeds along this axis over the United States were located over Wisconsin directly north of the High center over Mississippi. (See fig. 4.) Meanwhile, wind speeds were extremely weak over the South along the major east-west axis of the anticyclone. Considerable anticylonic shear existed between the westerly belt across the North and the virtually stagnant flow to the South. This shear, combined with anticyclonically curved contours in figure 4, resulted in pronounced anticyclonic vorticity over a broad area from northwest Mexico east-northeastward to the Middle Atlantic States (fig. 6). The strongest anticyclonic vorticity was centered just north of the High cell over western Tennessee. It is interesting to note that the area enclosed by the -1 vorticity line in figure 6 coincided almost exactly with the region enclosed by the $+5$ anomaly line in figure 4, showing a remarkable similarity between positive height anomalies and anticylonic vorticity over the United States. Perhaps most important is the fact that this area where 700-mb. heights and anticyclonic vorticity were at a maximum also closely coincided with the large area of predominantly light precipitation extending from New Mexico to the Lakes region shown in figure 2-B or Chart III–B.

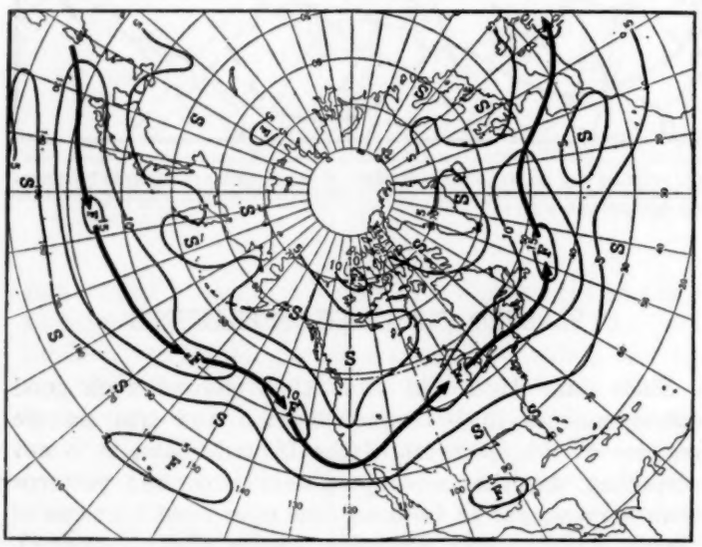

FIGURE 5.—Mean 700-mb. wind speeds (isotachs drawn at intervals of 5 m/sec) for May 30–June 28, 1953. Solid arrows indicate the average position of jet stream at this level. Relatively fast westerlies blew along the northern periphery of continental High cell centered over Mississippi. (See fig. 4.)

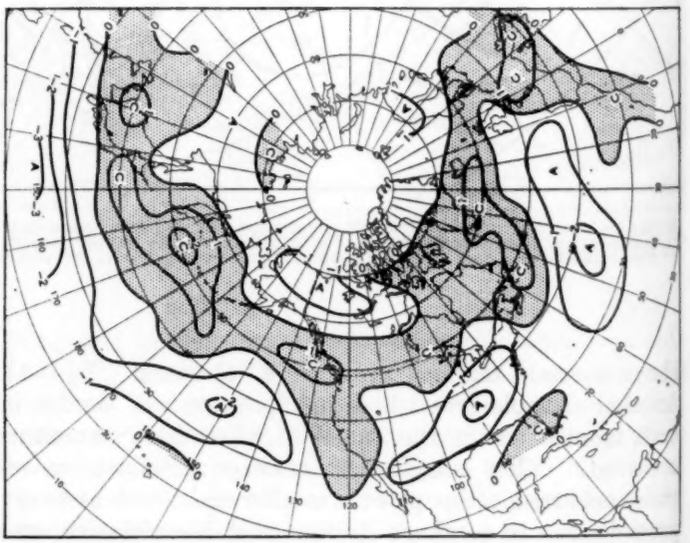

FIGURE 6.—Mean relative geostrophic vorticity at 700 mb. (in units of 10^{-6} sec^{-1}) for May 30–June 28, 1953. Areas of cyclonic vorticity are shaded and labeled "C" at centers of maximum vorticity. Centers of anticyclonic vorticity are labeled "A". Pronounced anticyclonic vorticity dominated much of the United States from the Southwest to the Northeast. This was associated with strong wind shear south of the jet shown in figure 5 and with anticyclonic curvature in the circulation around the High cell portrayed in figure 4.

Figure 7 and Charts XI and XV demonstrate that the well-developed mid-continent ridge, as well as other large-scale features of the circulation pattern, remained virtually unchanged up into the lower stratosphere. It is noteworthy, however, that at 200 mb. the High was centered in southeastern Mexico compared with its lower-level position over Mississippi at 700 mb. The axis of maximum wind speeds at 200 mb., which is also shown in figure 7, paralleled quite closely the axis at 700 mb. (fig. 5), but was generally slightly farther north from the west coast to the northern Plains. Maximum wind speeds in the 200-mb. jet over North America were located over California and Nevada. The highest value was about 32 m./sec., as much as five times as great as the speeds directly below at 700 mb. A secondary maximum was located near the Great Lakes, close to the maximum at 700 mb., but here speeds at 200 mb. were only about 2¼ times those at 700 mb. The High at 700 mb. (fig. 4) was located almost directly under the 200-mb. ridge where weak mean westerly winds of about 10 m./sec. were passing over it.

OTHER ASPECTS OF THE WEATHER AND CIRCULATION

Severe local storminess continued to dominate the weather news during the first half of June. A series of devastating tornadoes on the 8th and 9th caused the greatest loss of life and the most property damage. These were concentrated in eastern Michigan and northern Ohio on the 8th and in southeastern New Hampshire and central Massachusetts on the 9th. They occurred in connection with the eastward passage of a pronounced prefrontal squall line which in turn was associated with a deep Low which moved out of New Mexico, across Lake Superior, and eastward through southeastern Canada (Chart X). This was slightly to the south of the prevailing cyclone track shown in figure 8–B. In general most of the tornadoes in June were confined to the northern Border and central Plains States as they were in the last third of May. As pointed out last month by the author [3], the establishment of the continental anticyclone and the shifting of the main westerly belt to the northern United States early in the last decade of May brought an end to severe storminess in the South, but allowed continued storminess across the North.

Several cyclones formed or redeveloped east of the Continental Divide during June and moved north-northeastward through the northern Plains and Upper Lakes and then joined with the principal Canadian storm track (fig. 8–B or Chart X). Most of the cyclogenesis took place to the south of the mean jet stream axis at both 700 mb. and 200 mb. (figs. 5 and 7) where anticyclonic vorticity prevailed (fig. 6). Once formed, the cyclones

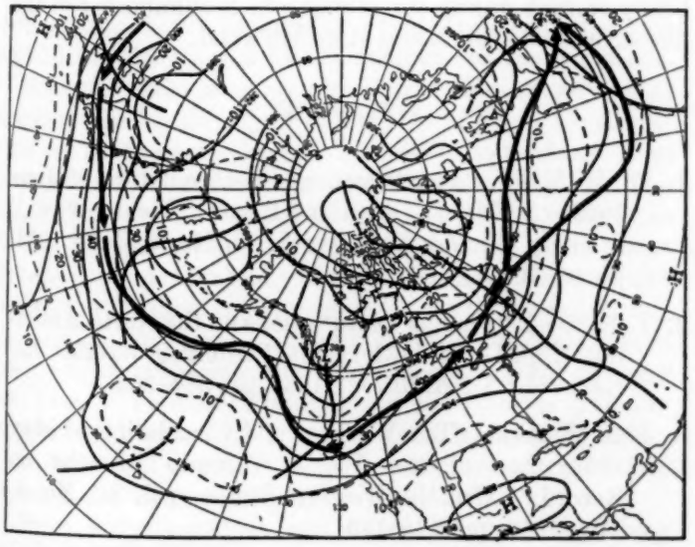

FIGURE 7.—Mean 200-mb. chart with contours (labeled in hundreds of feet) and isotachs (labeled in meters per second) for May 30–June 28, 1953. Note very great similarity in basic pattern to 700-mb. level (fig. 4). Solid arrows indicate the average position of jet stream, which corresponds closely with the position of 700-mb. jet over the United States (fig. 5).

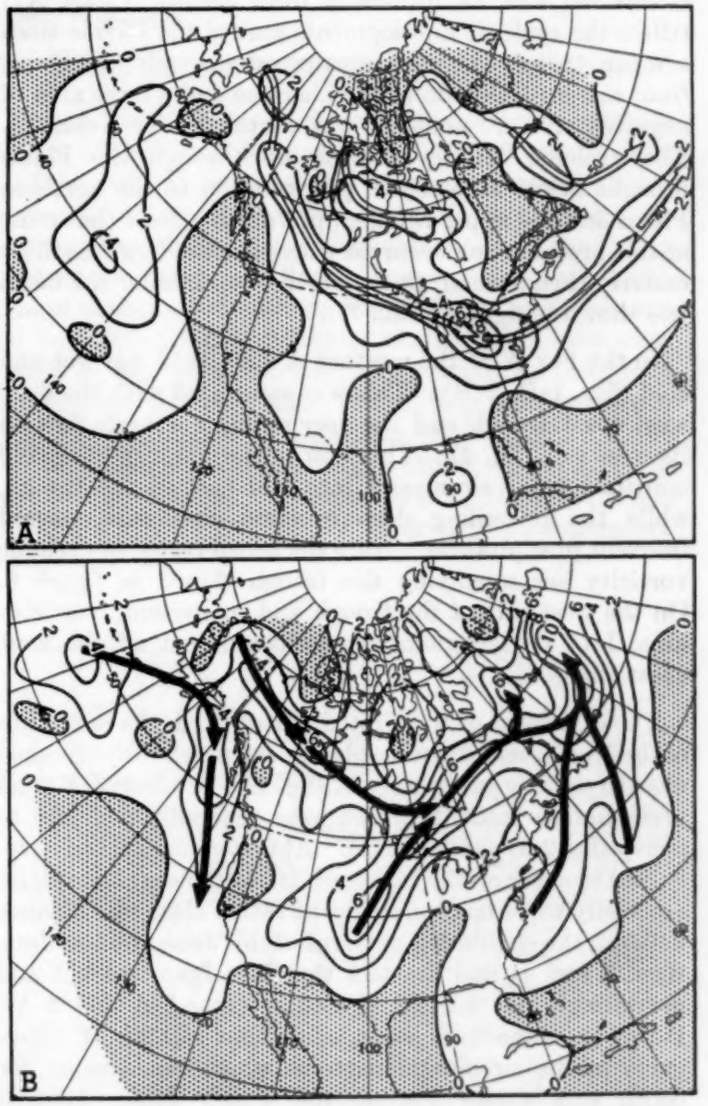

FIGURE 8.—Frequency of (A) anticyclone passages and (B) cyclone passages (within 5° squares at 45° N.) during June 1953. Well-defined anticyclone tracks are indicated by open arrows and cyclone tracks by solid arrows. Note well-defined anticyclone path from western Canada through Middle Atlantic States with maximum frequency in Ohio. Also noteworthy is frequent cyclonic development over Plains with track northward through Minnesota. Both cyclones and anticyclones were infrequent in the drought and heat wave area of the South Central States.

moved rapidly northward toward the center of cyclonic vorticity just north of Minnesota. Moreover they developed at a distance of some 1,000 to 1,200 miles to the east of the deeper-than-normal west coast trough. Such a large displacement between upper-level trough and sea-level cyclonic activity is frequently found in this area, but it is much larger than that normally occurring in other parts of the Northern Hemisphere. It is probably a result of both the land-sea temperature contrast, which is very pronounced over the West in June, and the topographic effects of the Rockies on the flow, which often damp out sea-level cyclones over the Plateau and create them east of the Continental Divide. If one examines the daily synoptic maps, the relationship between the west coast trough and the cyclones east of the Divide becomes more apparent. Sharp cold fronts moving across the West out of the trough provided perturbations from which new Lows formed east of the Divide. The mean sea level circulation and its departure from normal (Chart XI) reflect the cyclonic developments east of the Divide since a mean trough extended northward through the Plains from eastern Colorado to the Dakotas and a large area of negative pressure anomaly was centered over Nebraska. The cyclonic activity moving up through the Plains brought heavy amounts of precipitation to the northern Plains and the upper Mississippi Valley. Note that most of this precipitation occurred where surface flow was more easterly then normal, to the north of and under the mean jets shown in figures 5 and 7.

In the Far West the weather of June 1953 was wet and cold (figs. 1-B, 2-B). This was associated with the deep west coast trough and the very strong northerly flow on its west side (fig. 4). This flow pattern transported cold maritime polar air masses into and east of the trough, while the prevailing deep cyclonic circulation caused frequent precipitation. Note the broad region of cyclonic vorticity accompanying the trough shown in figure 6. On the west side of the trough and its cyclonic vorticity area, Low centers plunged southward just off the west coast (fig. 8-B).

The east coast of the United States (with the exception of the Northeast) experienced temperatures which averaged near to slightly below normal (fig. 1-B or Chart I-B) and precipitation amounts which were generally moderate to heavy (fig. 2-B or Chart III). At first glance this relatively cool weather on the east coast is not too easy to explain, especially when one considers the rather close resemblance between the circulation patterns of this June and last June (figs. 3 and 4) and the fact that last June was hot and prevailingly dry on the east coast (figs. 1-A and 2-A). However, there were some subtle, but significant differences in the circulation patterns which can account for cooler and wetter weather this June. First, the east coast trough was considerably farther west, south of 40° N., trailing back across southern Florida and into the Gulf of Mexico this month, so that flow along the east coast was more northerly than normal and more meridional than it was last June. Second, heights near Hudson Bay were slightly above normal this June whereas they were markedly below normal last June, so that the westerlies across southeastern Canada were not as strong as last June; and there were even several short periods in the first half of the month when the westerlies were very weak. As a result Canadian polar air was able to penetrate the entire east coast on several occasions accompanied by frontal rainfall and showers. Figure 8-A shows that the major anticyclone path across the east coast was through the Middle Atlantic States. Most of these Highs formed as breakoffs from the mean Highs in the Pacific or northern Canada (Chart XI) and moved southeastward across the Lakes to the Atlantic Coast, bringing fresh supplies of polar air into the east coast. Cyclogenesis occurred several times just along the east coast in association with the coastal trough (Chart X). This cyclone track extended northeastward into a region of strong cyclonic vorticity aloft near Newfoundland, and there joined with the Canadian storm track to form a region of very high frequency of migratory storms south of Greenland (figs. 6 and 8-B).

In conclusion a word may be said about the disastrous floods which occurred in Japan near the end of June. These floods were termed unprecedented in modern history with a death toll of over 1,000, more than 60,000 people homeless, and widespread property damage. The monthly mean circulation pattern in that area (fig. 4) consisted of a trough along the Asiatic east coast which was slightly deeper than normal and a subtropical High cell south of Japan which was much stronger than normal. It is believed that the broad abnormally strong southwesterly flow over the China Sea and Japan, transporting copious amounts of moist air from Southeast Asia, led to frequent heavy rainfall during the month which culminated in the disastrous flood conditions at month's end.

REFERENCES

1. W. H. Klein, "The Weather and Circulation of June 1952—A Month with a Record Heat Wave," *Monthly Weather Review*, vol. 80, No. 6, June 1953, pp. 99–104.
2. T. R. Reed, "Further Observations on the North American High-Level Anticyclone," *Monthly Weather Review*, vol. 65, No. 10, Oct. 1937, pp. 364–366.
3. J. S. Winston, "The Weather and Circulation of May 1953—One of the Worst Tornado Months on Record," *Monthly Weather Review*, vol. 81, No. 5, May 1953, pp. 135–140.

LOW LEVEL WARM AIR ADVECTION, JUNE 8-9, 1953

GEORGE C. HOLZWORTH AND CHARLES F. THOMAS

WBAN Analysis Center, U. S. Weather Bureau, Washington, D. C.

INTRODUCTION

Meteorologists have long realized the importance of warm air advection in the lower levels of the atmosphere—especially in relation to regions of active weather such as cloudiness and precipitation [1, 2]. Intimately tied to these regions of warm air advection and weather are fields of vertical motion and areas of surface pressure change. The effect of warm air advection in an air column contributing to a surface pressure fall and cold air advection contributing to a pressure rise is well understood [3]. However, in some discussions of temperate zone weather, warm and cold air advection are treated with reference to the usually observed attendant advection of high, cold and low, warm tropopauses, respectively. For instance, when it is pointed out that indicated warm air advection in the lower levels (500 mb. or lower) will likely lead to a buildup of higher surface pressures, what is really implied is that the lower warming will be more than balanced by the advection aloft of a high, cold tropopause. The upper level cold air advection is expected to more than compensate the lower warm air advection—there will be a density increase—and surface pressures will rise. Cooling in an air column contributes to a surface pressure rise and warming contributes to a fall. In all discussions the terminology should be consistent with the actual processes as well as with what is finally observed as the net result.

Since thickness lines are also isotherms of mean virtual temperature for the layer, the regions of warm air advection are those where the flow is against the thickness lines and directed from higher toward lower values. The spacing of the thickness lines depends on the magnitude of the thermal wind, which simply is the wind shear between the bottom and the top of the layer; the stronger the shear, the greater the gradient. At the same latitude geostrophic flow on a constant pressure surface depends on the contour spacing; the closer the spacing, the stronger the flow. Therefore, the indicated advection is inversely proportional to the quadrangular areas bounded by thickness lines and contours of a constant pressure surface through the thickness layer.

From a study of low level warm air advection during the period June 8–9, 1953, this paper presents some thickness and pressure change relationships, and, employing the displacement of thickness lines, some simple computations of vertical motion are made. The paper attempts to describe a clear and consistent picture of the general density changes occurring below 500 mb. and to reason the changes that must be taking place above 500 mb. to be mutually consistent with observed sea level pressure changes.

THICKNESS AND PRESSURE CHANGE RELATIONSHIPS

Figure 1 is a composite chart of the 1000-mb. contours and the 1000-500-mb. thickness lines for 0300 GMT on June 8, 1953. At this time the area of strongest warm air advection is indicated near the center of the chart by the concentration of the small quadrangular areas bounded by contours and thickness lines. Figure 2 is a composite 12-hour change chart, showing the 1000-mb. height change and the 1000-500-mb. thickness change from 1500 GMT, June 7 to 0300 GMT, June 8. Since thickness lines may be considered as fairly conservative, their movement can be attributed mainly to advection [4]. In figure 2 the area of positive thickness change shows where warming has actually occurred. A change of about 66½ feet in the 1000-500-mb. layer is equal to a mean virtual temperature change of 1° C.

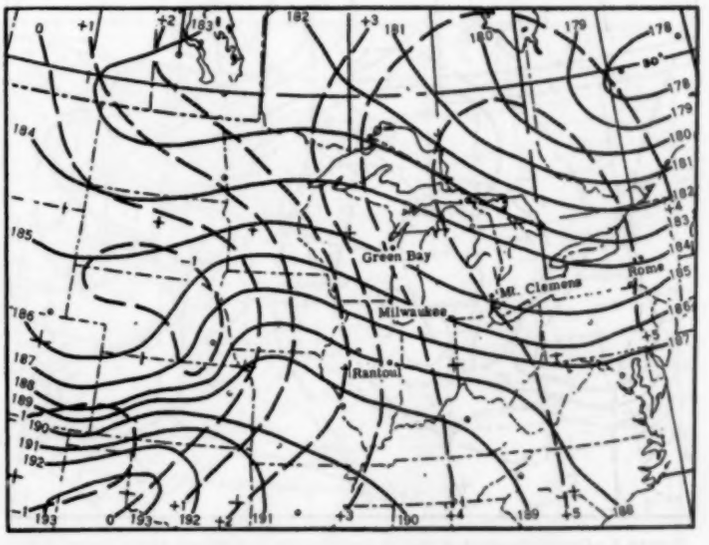

FIGURE 1.—Composite chart of 1000-500-mb thickness (solid lines) and 1000-mb. height (dashed lines) for 0300 GMT, June 8, 1953. Values are in hundreds of feet.

The actual contribution to the surface pressure fall by warming in the layer may be closely approximated from elementary considerations. If the 500-mb. height does not change and the 1000-mb. height falls, the 1000-500-mb. layer gets thicker (less dense) and contributes to a surface pressure fall. In this case the contribution to the surface pressure fall comes entirely from below 500 mb. However, if the 500-mb. height also falls, but not as much as the 1000-mb. height fall, then the contribution *of this layer* to the surface pressure fall is reduced. Since thickness changes are transmitted downward as pressure changes it is possible to compute the contribution of the particular layer to the surface pressure change. For instance, at Duluth, Minn. at 0300 GMT, June 8 (fig. 2) the 1000-500-mb. thickness has increased 200 feet, the 1000-mb. height has decreased 250 feet, and so the 500-mb. height has decreased 50 feet. Near sea level, pressure decreases with height at the rate of about 1 mb. per 28 feet, U. S. Standard Atmosphere. Since the 1000-mb. height fell 250 feet, the surface pressure fell about 9 mb. but since the 1000-500-mb. layer thickened only 200 feet, the contribution of this layer to the surface pressure fall is 4/5 or 80 percent. The remaining 20 percent must have come from above 500 mb. A slight contribution may come from below 1000 mb. but for practical purposes this is negligible.

Along the eastern edge of the surface Low center (fig. 1) only slight warming is occurring in the 1000-500-mb. layer (fig. 2). But in this same zone rather pronounced 1000-mb. height falls are taking place. As a matter of fact, just a little farther east is located the center of 1000-mb. height fall, enclosed within a −300-foot isallohypse, and through this center runs the relative isallohypse of 100-foot increase in thickness of the 1000-500-mb. layer. Thus, in this area the decrease in density of the 1000-500-mb. layer accounts for only about one-third of the observed sea level pressure fall. Consequently the main contribution of density decrease to sea level pressure fall must come from above the 500-mb. level.

Eastward of the main center of 1000-500-mb. thickness increase (fig. 2) is the area where warming (increased thickness) exactly balances the observed sea level pressure fall; here is also the zone where the 500-mb. height change is zero. This does not mean that density changes are not taking place above 500 mb., undoubtedly they are, but they are counterbalancing each other so that the net effect at 500 mb. and below is zero.

Farther eastward toward the High center, but in the region of positive 1000-500-mb. thickness change and negative 1000-mb. height change, low level warming accounts for a greater pressure fall than is actually observed; density increase above 500 mb. must be occurring to compensate the excess density decrease below. Near the western edge of the High center this effect is even

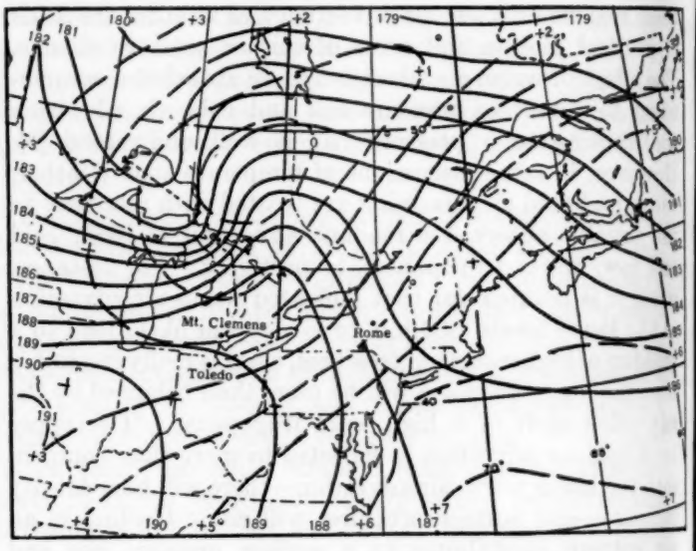

FIGURE 3. Composite chart of 1000-500-mb. thickness and 1000-mb. height for 1500 GMT, June 8, 1953.

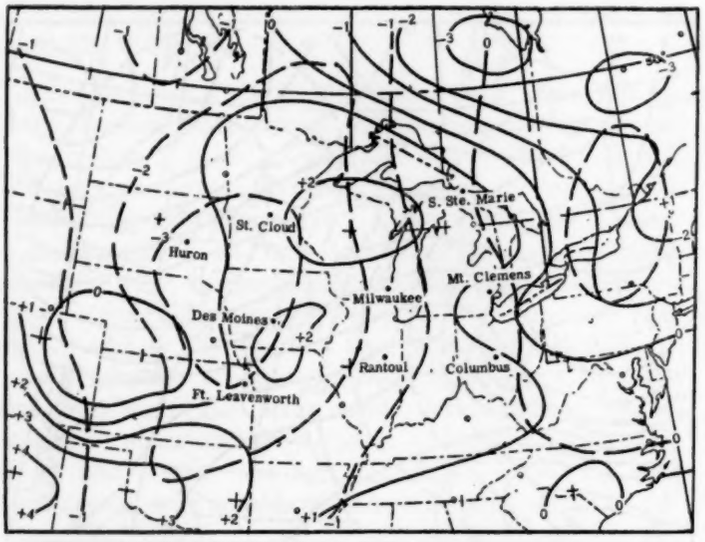

FIGURE 2.—Composite chart of 12-hour change of the 1000-500-mb. thickness (solid lines) and 1000-mb. height (dashed lines) from 1500 GMT, June 7 to 0300 GMT, June 8. Values are in hundreds of feet.

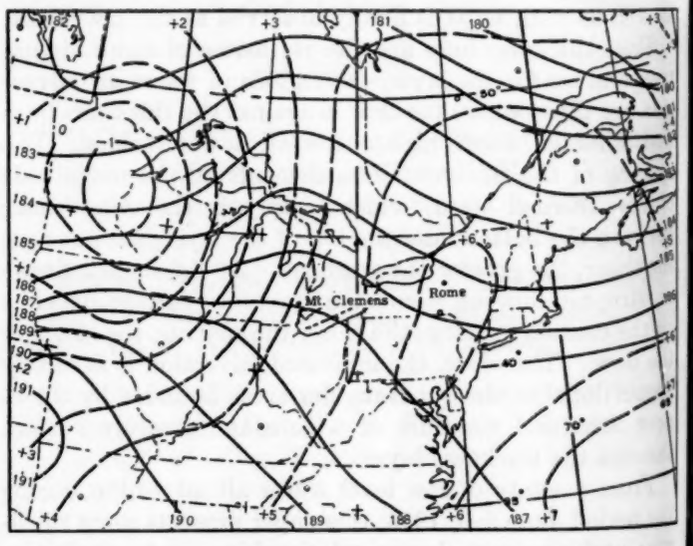

FIGURE 4.—Composite chart of 1000-500-mb. thickness and 1000-mb. height for 0300 GMT, June 9, 1953.

better illustrated. For here the sea level pressure is rising in spite of warming in the 1000-500-mb. layer.

Through the High center the thickness change is small and negative, and contributes slightly to the observed rise in surface pressure. Along the eastern edge of the High center the increase in density of the 1000-500-mb. layer becomes the main source of rising sea level pressure, and is balanced by a density decrease above 500 mb.

Thus, in this case one is led to the following picture of the balance of density decrease and increase above and below 500 mb. in contributing to sea level pressure change: Along the eastern edge of the Low center warming occurs below 500 mb., but the main contribution of density decrease to sea level pressure fall comes from above 500 mb. About half way from Low to High, low level warming completely accounts for the observed sea level pressure fall; the net effect from above 500 mb. is zero. A little farther east, low level warming accounts for more pressure fall than is observed so increased density above 500 mb. occurs. Near the High center low level cooling becomes most effective and therefore the amount of density increase at upper levels diminishes.

Figures 3 and 4 show how the areas of indicated warm air advection moved from southwest to northeast, and figures 5 and 6 show the 12-hour changes of 1000-500-mb.

TABLE 1.—*Relationship of 1000-500-mb. thickness change to surface pressure and 500-mb. height changes*

1500 GMT, June 7, to 0300 GMT, June 8, 1953

Station	ΔH_{1000}	$\Delta Z_{1000-500}$	ΔH_{500}	Δp
	Feet	*Feet*	*Feet*	*Millibars*
Huron, S. Dak	−320	+70	−250	−11.5
St. Cloud, Minn	−335	+175	−160	−12
Sault Ste. Marie, Mich	−20	+160	+140	−1
Des Moines, Iowa	−305	+210	−95	−11
Milwaukee, Wis	−150	+160	+10	−5
Mount Clemens, Mich	−25	+55	+30	−1
Fort Leavenworth, Kans	−285	+145	−140	−10
Rantoul, Ill	−140	+180	+40	−5
Columbus, Ohio	−20	+105	+95	−1
0300 GMT, June 8 to 1500 GMT, June 8, 1953				
Moosonee, Ontario	−60	+300	+240	−2
International Falls, Minn	−320	−80	−400	−11.5
Kapuskasing, Ontario	−165	+320	+155	−6
Lake Dore, Quebec	+105	+425	+530	+4
Green Bay, Wis	−310	+50	−260	−11
Alpena, Mich	−210	+165	−45	−7.5
Montreal, Quebec	+110	+235	+345	+4
Madison, Wis	−225	+25	−200	−8
Mount Clemens, Mich	−100	+205	+105	−3.5
Rome, N. Y	+105	+145	+250	−4
1500 GMT, June 8 to 0300 GMT, June 9, 1953				
Moosonee, Ontario	−350	−40	−390	−12.5
Alpena, Mich	−265	+40	−225	−9.5
Montreal, Quebec	−230	+155	−75	−8
Caribou, Maine	−60	+120	+60	−2
Milwaukee, Wis	+50	+100	+150	+2
Mount Clemens, Mich	−210	+150	−60	−7
Buffalo, N. Y	−250	+210	−40	−9
Rome, N. Y	−225	+135	−90	−8
Portland, Maine	−20	+85	+65	−1.5

ΔH_{1000}=12-hr. change in height of 1000-mb. level
ΔH_{500}=12-hr. change in height of 500-mb. level
$\Delta Z_{1000-500}$=12-hr. change in 1000 to 500-mb. thickness
Δp=12-hr. change in sea level pressure

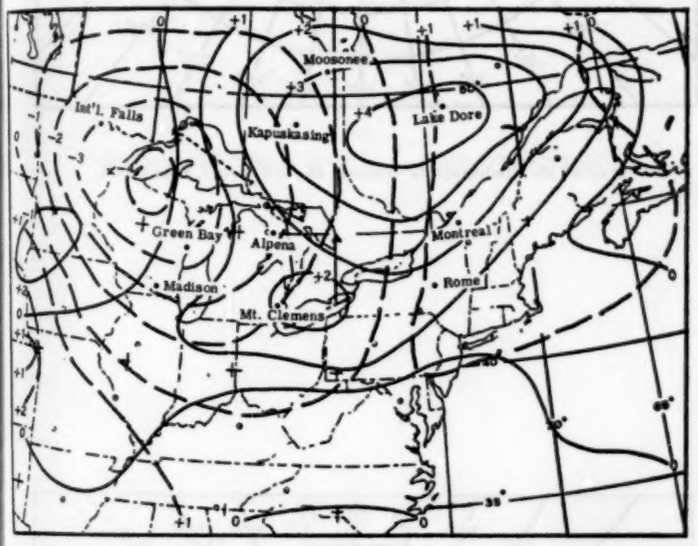

FIGURE 5.—Composite chart of 12-hour change of 1000-500-mb. thickness and 1000-mb. height from 0300 GMT to 1500 GMT, June 8, 1953.

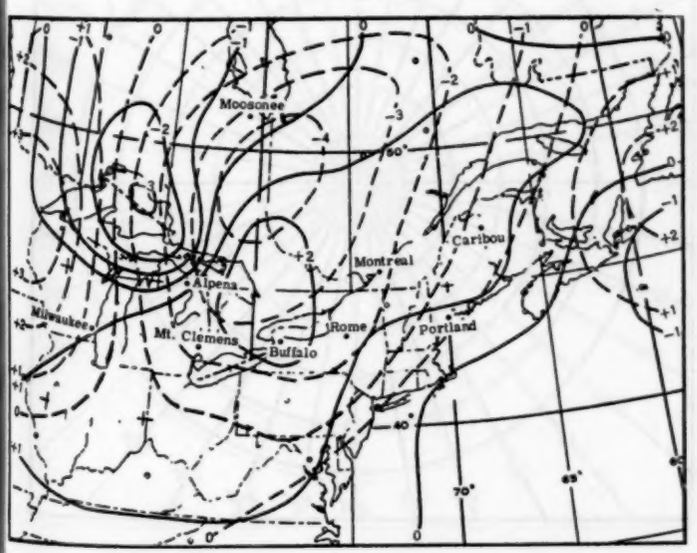

FIGURE 6.—Composite chart of 12-hour change of 1000-500-mb. thickness and 1000-mb. height from 1500 GMT, June 8 to 0300 GMT, June 9, 1953.

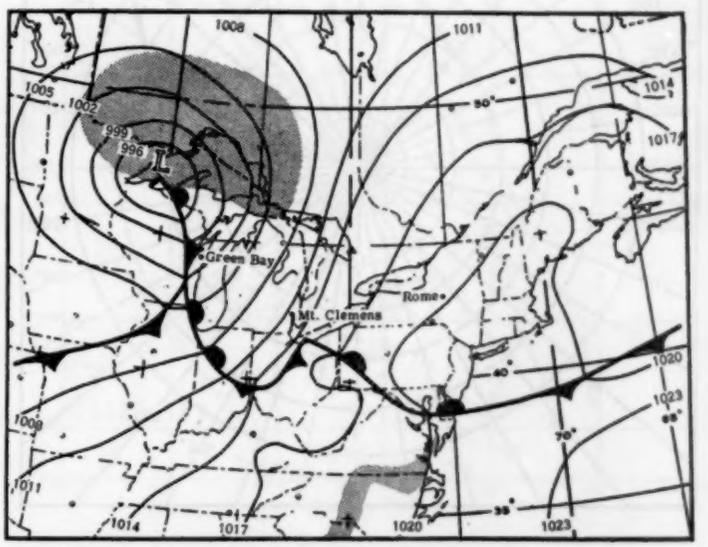

FIGURE 7.—Sea level weather chart for 1830 GMT, June 8, 1953. Shading represents the area where precipitation is occurring.

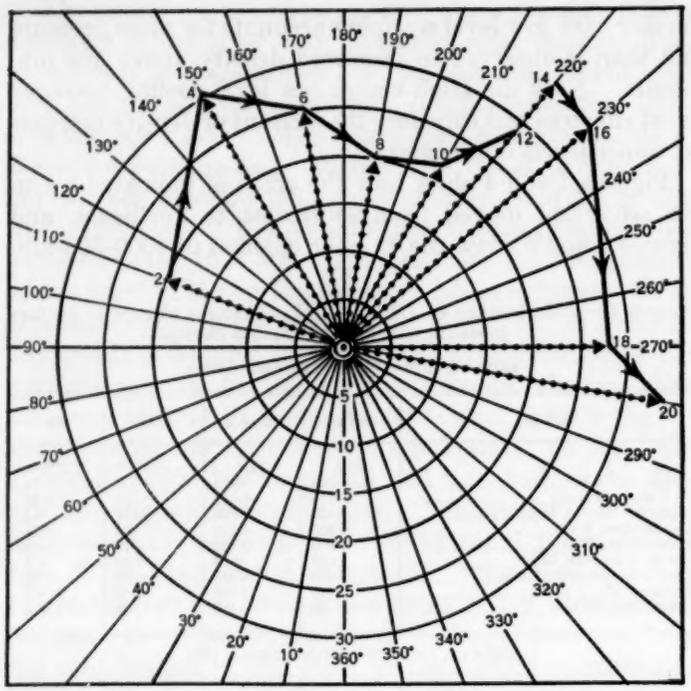

FIGURE 8.—Hodograph for Milwaukee, Wis., at 0300 GMT, June 8, 1953. The dotted vector is the observed wind in knots. The numbers on the periphery indicate the direction from which the wind is blowing. The figure near the vector head is the elevation in thousands of feet. The heavy vectors, indicating warm advection, are the thermal or shear vectors. For clarity the direction of the shear is shown along only some of the thermal vectors.

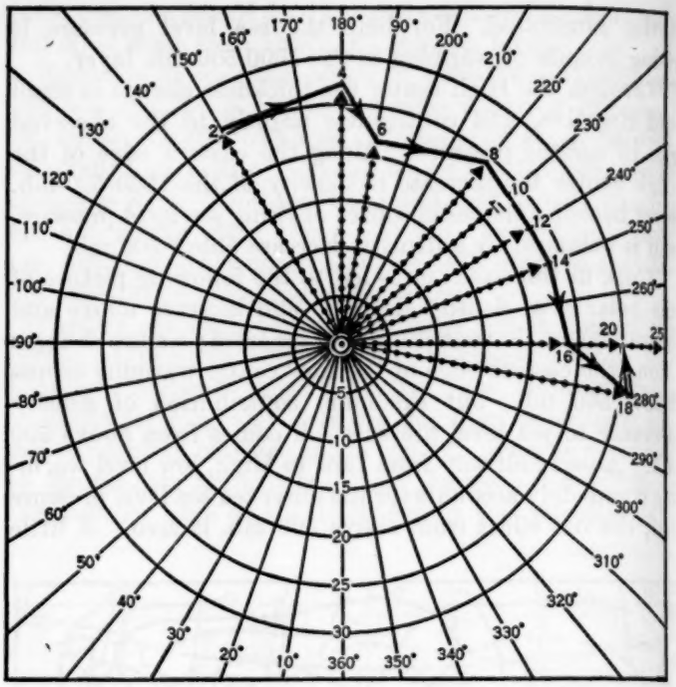

FIGURE 10.—Hodograph for Rantoul, Ill., at 0300 GMT, June 8, 1953.

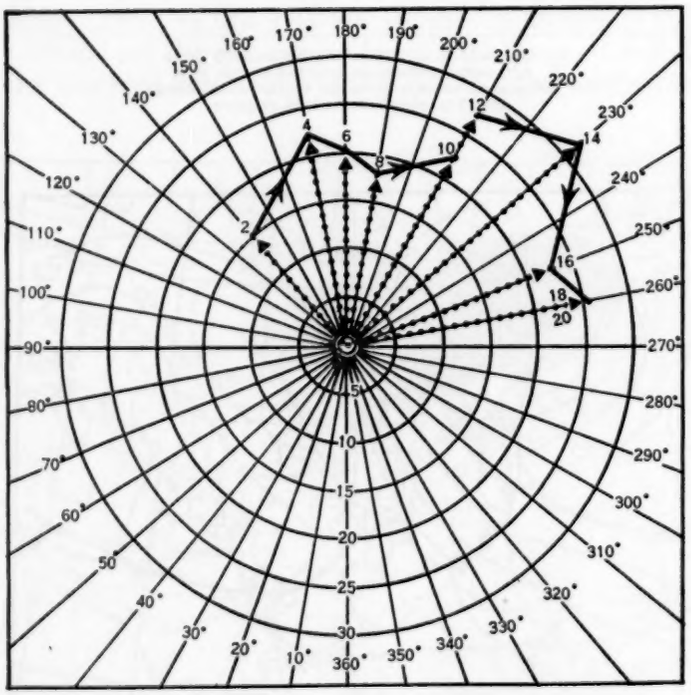

FIGURE 9.—Hodograph for Green Bay, Wis., at 0300 GMT, June 8, 1953.

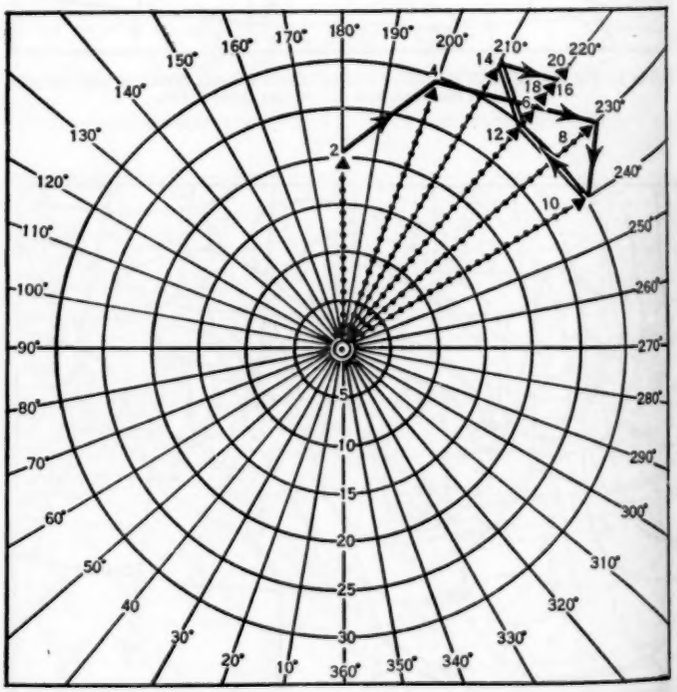

FIGURE 11.—Hodograph for Mount Clemens, Mich., at 1500 GMT, June 8, 1953.

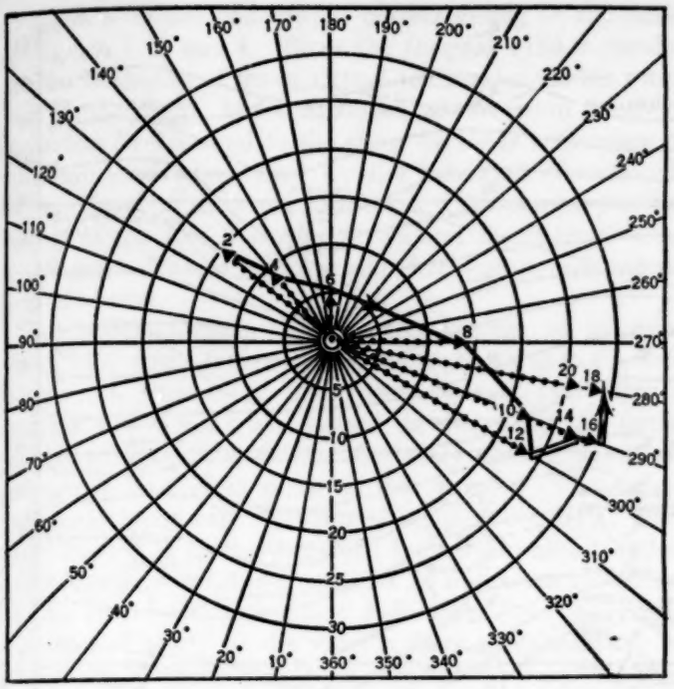

FIGURE 12.—Hodograph for Rome, N. Y., at 1500 GMT, June 8, 1953.

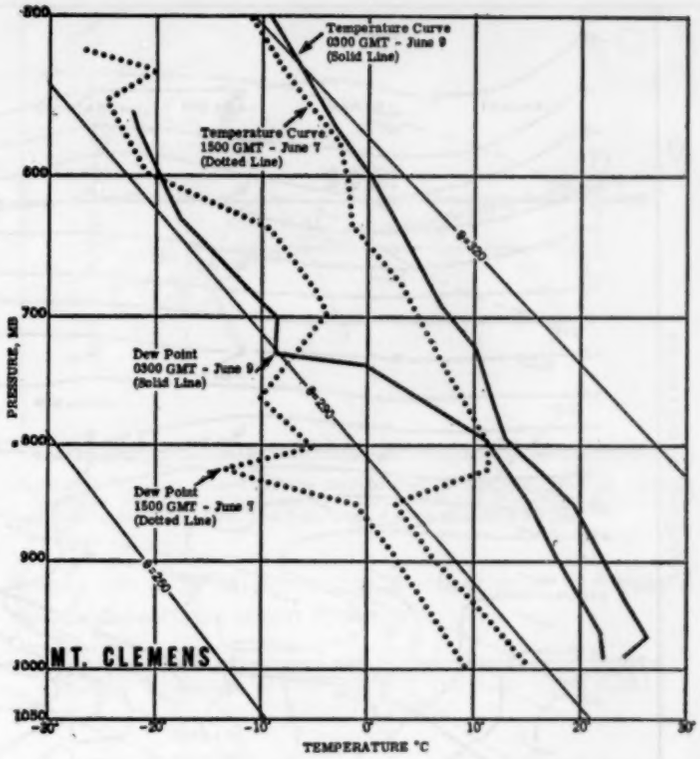

FIGURE 14.—Upper air soundings over Mount Clemens, Mich., at 1500 GMT, June 7 and 0300 GMT, June 9, 1953.

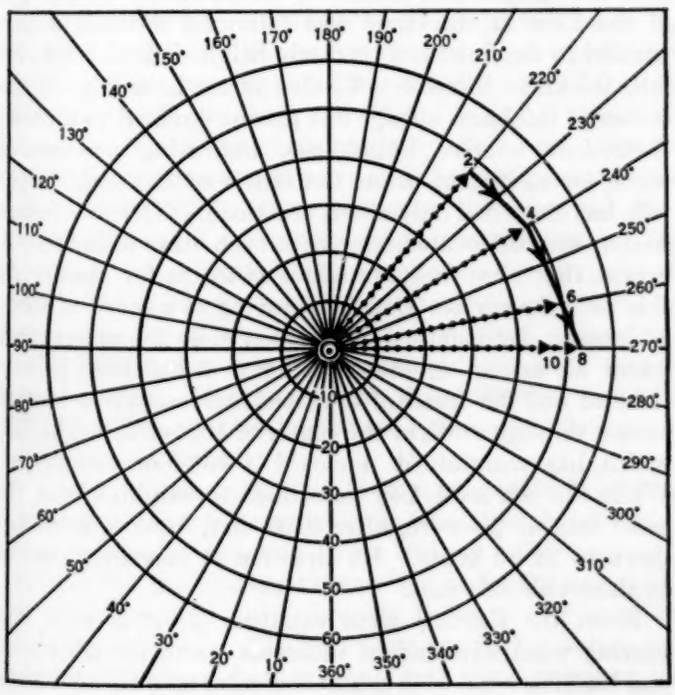

FIGURE 13.—Hodograph for Toledo, Ohio, at 0300 GMT, June 9, 1953.

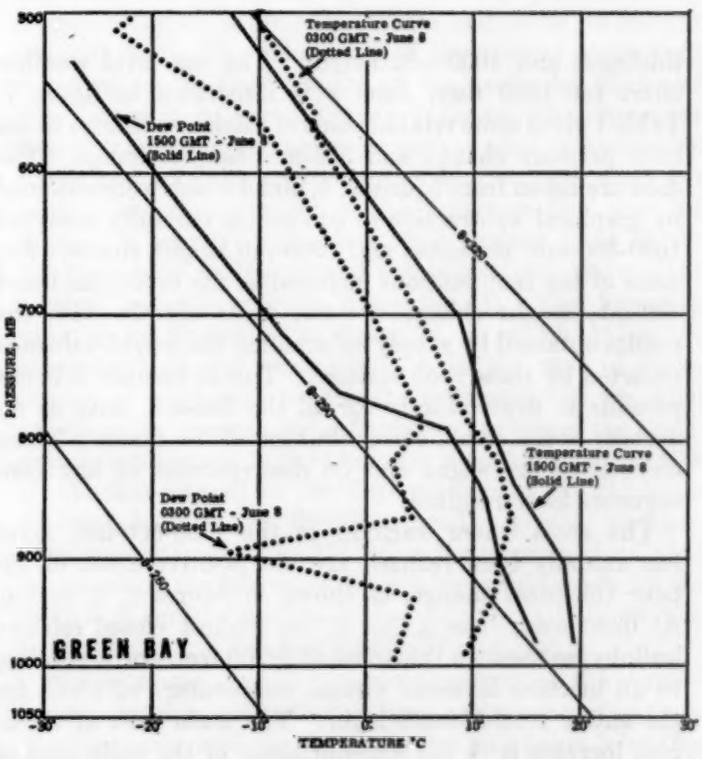

FIGURE 15.—Upper air soundings over Green Bay, Wis., at 0300 GMT and 1500 GMT, June 8, 1953.

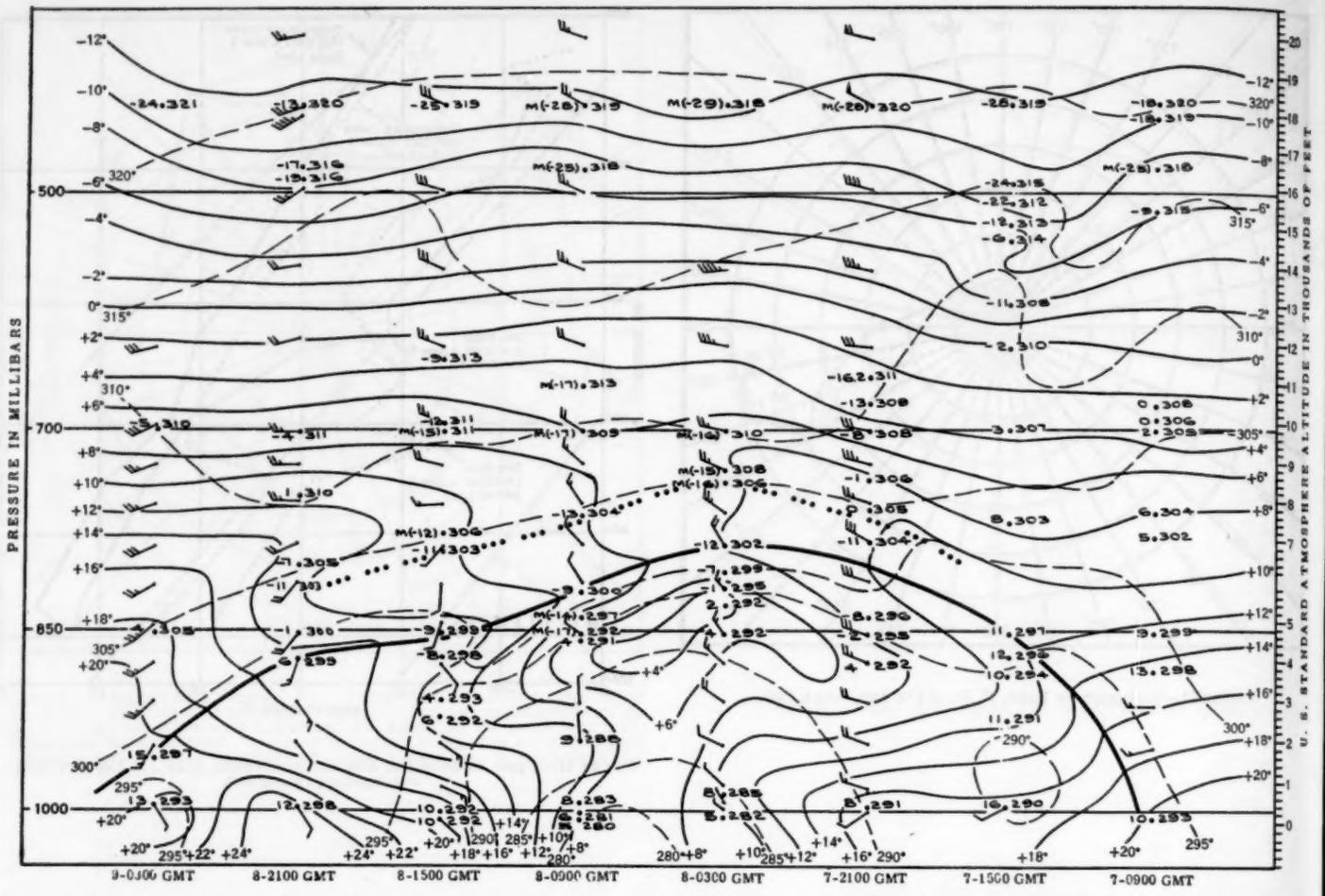

FIGURE 16.—Six-hourly time cross section over Mount Clemens, Mich. For clarity only the potential and dew point temperatures are plotted. The front is indicated by the heavy solid line, the subsidence inversion by the dotted line, the isotherms in ° C. by the light solid lines, and the potential temperature isotherms in ° A. by the dashed lines.

thickness and 1000-mb. height. The sea level weather chart for 1830 GMT, June 8 is illustrated in figure 7. Table 1 gives some relationships of thickness change to sea level pressure change and 500-mb. height change. The data are taken from figures 2, 5, and 6 which were obtained by graphical subtraction of succeeding carefully analyzed 1000-500-mb. thickness and 1000-mb height charts. For some of the raob stations included in the table, the listed 500-mb. height changes do not agree exactly with the results obtained by simply subtracting the height values as reported by these raob stations. This is because it is not possible to draw exactly for all the 500-mb. data as reported; some small corrections must be made. These corrections are slight and no discrepancies of any consequence have resulted.

The areas where warming in the 1000-500-mb. layer has actually been realized are the positive areas of 12-hour thickness change, as shown in figures 2, 5, and 6. At 0300 GMT, June 8 (fig. 2) the highest closed relative isallohypse shows a thickness of +200 feet, corresponding to an increase in mean virtual temperature of 3° C. for the entire 1000-500-mb layer. The main area of thickness increase is to the east-northeast of the main area of 1000-mb. height fall (surface pressure fall). The center of the Low at this time was following a track almost parallel to the line from 1000-mb. height falls to 1000-500-mb. thickness increase. Twelve hours later (fig. 5) the center of thickness change has almost doubled to a closed +400-foot relative isallohypse, indicating pronounced warm air advection, while the center of 1000-mb. height falls has deepened only about one third. The two change centers are still located relative to each other as in figure 2, except that now they are about twice as far apart. At this time the surface Low was moving at a speed of about 40 knots. By 0300 GMT, June 9 (fig. 6) the pronounced warm air advection shown in figure 5 has been greatly reduced and the center of thickness increase is now located almost directly south of the center of 1000-mb. height fall, which has maintained a closed —400-foot isallohypse. While the sea level Low continued to exhibit about the same central pressure, after 0300 GMT, June 9, it slowed down to 25–30 knots. Its direction of movement veered to almost directly east.

From the thermal wind equation [3] it is seen that veering wind with height indicates warm air advection, and backing wind with height indicates cold air advection.

Figures 8–13 are hodographs corresponding to the times of figures 1, 3, and 4. Since the thermal wind is parallel to the isotherms of mean virtual temperature, with warm air to the right, the component of the wind *at either bounding level* normal to the shear vector is a measure of the indicated advection. Or the indicated advection is proportional to the areas of the triangles composed of the winds at the two bounding levels and the thermal wind (or shear). The hodographs all indicate pronounced warm air advection.

At Mount Clemens, Mich., the amount of warming from 1500 GMT, June 7, when the station was in the cold air at the surface, to 0300 GMT, June 9, just after a surface warm front had passed, is shown by the upper air soundings in figure 14. Certainly, strong warm air advection has taken place at this station. The superadiabatic lapse rate between 850 and 800 mb. at 0300 GMT, June 9, is interesting both from warm air advection considerations and the occurrence of numerous tornadoes in the area beginning about 2330 GMT, June 8. While no detailed study of the various factors contributing to the cause of these disastrous storms was made for this paper, it is the opinion of the writers and other members of the WBAN Analysis Center staff that strong warm air advection in the lower levels did play a part in the genesis of these tornadoes.

The upper air soundings over Green Bay, Wis., at 0300 GMT and 1500 GMT, June 8 (fig. 15) also show warming in the lower levels. At 0300 GMT Green Bay was well into the cold air; at 1500 GMT a surface occlusion was located just west of the station. The hodograph for Green Bay at 0300 GMT, June 8 is shown in figure 9.

A 6-hourly time cross section over Rome, N. Y., is shown in figure 16. At the beginning of the cross section, 0900 GMT, June 7, a cold front was approaching Rome, followed by a cold dome, and at the end of the cross section a warm front was approaching the station. Below the front the cold core was over Rome at about 0600 GMT, June 8. Above the front, generally, warm air advection was occurring from 1500 GMT, June 7 to 0900 GMT, June 8. The lowest 1000-500-mb. thickness value occurred about 0600 GMT, June 8. From the figure it is apparent that the main advection below 500 mb. took place below about 750 mb. The 1000-mb. height continued to rise, even after the cold core had passed, until it reached a maximum value of 610 feet (sea level pressure, 1022 mb.) at 1500 GMT, June 8. It appears that this continued rise after 0600 GMT, June 8 must have been due to a density increase above the 500-mb. layer.

Several of the soundings exhibited double inversions. The lower one was caused by the front and the upper one was rather dry, and was taken to be a subsidence layer formed by the sinking motion of the cold dome. This inversion appears very abruptly between 1500 GMT and 2100 GMT, June 7. The cold front was rather active, producing numerous showers along both sides of the surface front. As soon as this active weather zone had passed, the subsidence inversion appeared.

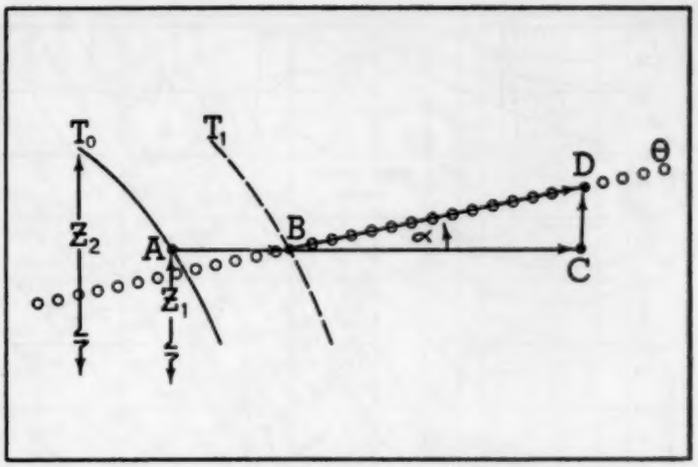

FIGURE 17.—Diagram illustrating the method used in computing vertical velocities. (See text.) T_0 and T_1 are thickness profiles at times T_0 and T_1 respectively. Z_1 and Z_2 are thickness values. The open-dotted line, θ, is an isentropic surface.

SOME SIMPLE COMPUTATIONS OF VERTICAL VELOCITIES

As stated previously, the regions of indicated warm air advection are those where the flow within a thickness layer is from higher to lower thickness values and therefore has a component against the thickness lines. However, it is seldom that the thickness lines move with the speed of the component normal to them. Rather, the thickness lines are considered to move with the speed of the front behind which they lie, 60 to 80 percent of the normal component for warm fronts and 70 to 90 percent for cold fronts [5]. That part of the normal component in excess of the displacement of the particular thickness lines, since it is directed toward denser air, represents flow upward along an isentropic surface until condensation is reached. If the component of the normal wind not used in the displacement of the thickness line, and the slope of a representative isentropic surface (that of the front) parallel to the normal component are known, the vertical velocity may be computed [5]. The foregoing principle is illustrated in figure 17, in which $\overline{AC}$ is the component of the mean wind or, in the case of linear change of wind with height, the component of the wind at either the upper or lower bounding surface of the thickness, taken normal to the thickness line; $\overline{AB}$ is the portion of $\overline{AC}$ that is used in the displacement of the thickness Z_1 from A to B; the thickness profile (greatly exaggerated) moves from T_0 to T_1; $\overline{BC}$ is the portion of $\overline{AC}$ that moves along the isentrope, θ; α is the angle made by the isentropic surface and the horizontal; and $\overline{CD}$ is the vertical velocity. From the figure $\overline{CD}=\overline{BC}\tan\alpha$.

Figure 1 was used in the computations of the components normal to the thickness lines. By comparing these displacements with the thickness chart 12 hours later (fig.

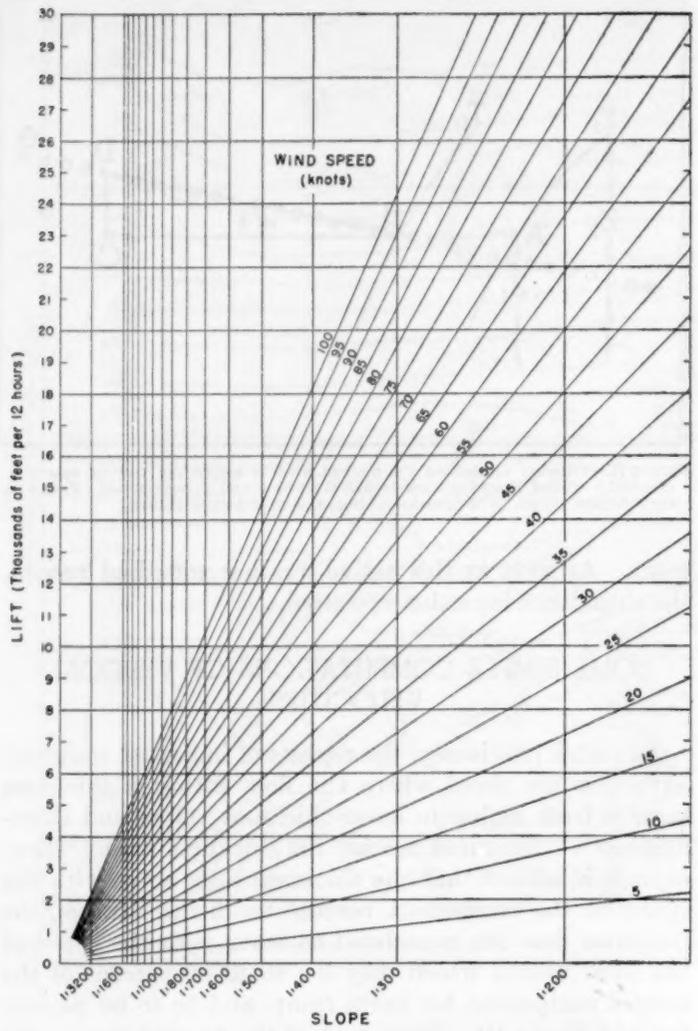

FIGURE 18.—Graph of the amount of lift in thousands of feet per 12 hours (ordinate), given the slope of the isentropic surface (abscissa) and the component of the normal wind (in knots) that is not accounted for by the movement of thickness lines. If the isentropic surface slope is negative, a particle will undergo subsidence.

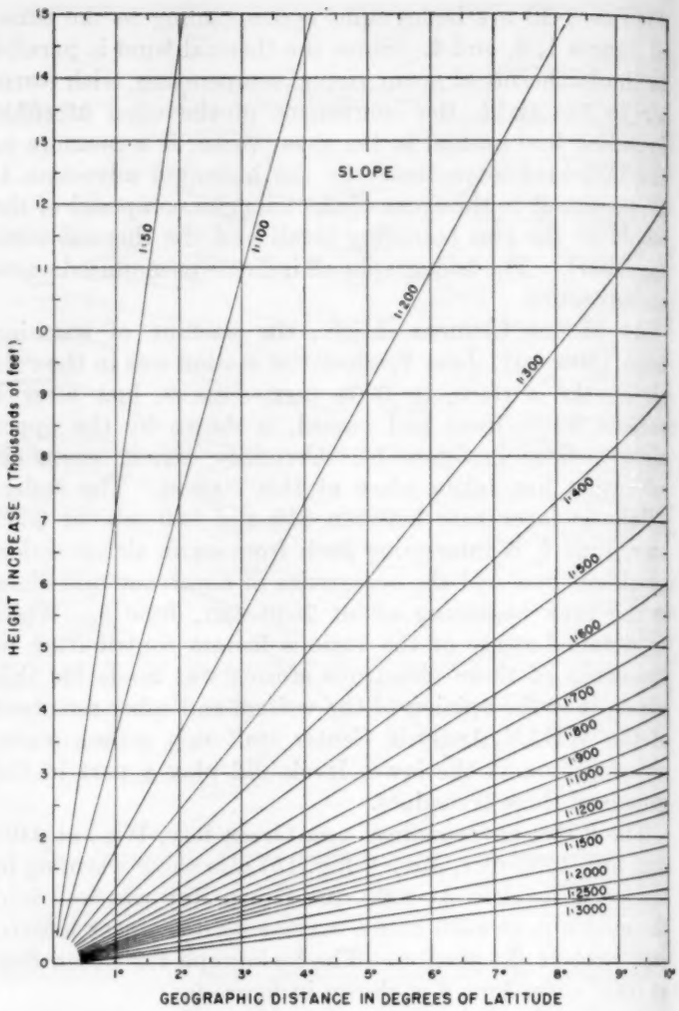

FIGURE 19.—Graph giving the slope of an isentropic surface, given the distance in degrees of latitude between two points (abscissa) and the difference in height in feet of the isentropic surface between these two points (ordinate). If the height of the isentropic surface decreases along the positive direction between two points, then the slope is negative.

3), the normal components that are not accounted for by the observed movements are obtained. Each "left over" component is then multiplied by the slope of the isentropic surface normal to the thickness line, and yields the vertical velocity. Figure 18 gives the amount of 12-hour lift in feet from the known values of isentropic slope (see fig. 19) and component normal to thickness lines that is not accounted for by displacement of the thickness lines. The 299° A. isentropic chart for 0300 GMT, June 8 is shown in figure 20, which also shows the advection arrows obtained from mean flow against 1000-500-mb. thickness lines.

The correlation between precipitation and vertical motion from 0300 GMT to 1500 GMT, June 8 is illustrated in figure 21. Figure 22 is a 299° A. isentropic chart for 1500 GMT, June 8. It is interesting to note that wherever warm air advection (thin arrows) is occurring the mean flow arrows are moving upslope along the isentropic surface, and where cold air advection (heavy arrows) is taking place the arrows are moving downslope. The correlation between precipitation and vertical motion from 1500 GMT, June 8 to 0300 GMT, June 9 is illustrated in figure 23.

At 1500 GMT, June 8 (fig. 3) rather pronounced warm air advection was indicated around the eastern periphery of the Low center. But 12 hours later (fig. 4) the cold front had swept into this area moving the thickness lines to the south. Therefore, the components of the wind normal to the thickness lines at 1500 GMT, June 8, that cannot be accounted for by advection of the thickness lines to their positions 12 hours later, are the normal components plus the speed of the southerly movement of the lines. This results in strong components, which yield rather high vertical velocities around the eastern edge of the Low center (fig. 23). Such values are in agreement with the well-founded theory of horizontal convergence around Low centers.

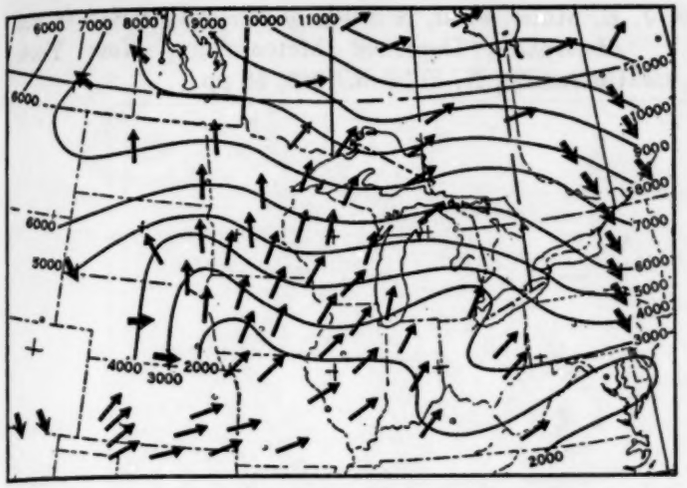

FIGURE 20.—229° A. isentropic chart for 0300 GMT, June 8, 1953. Warm and cold air advection, from considerations of mean flow against thickness lines, is indicated by the thin and heavy arrows, respectively.

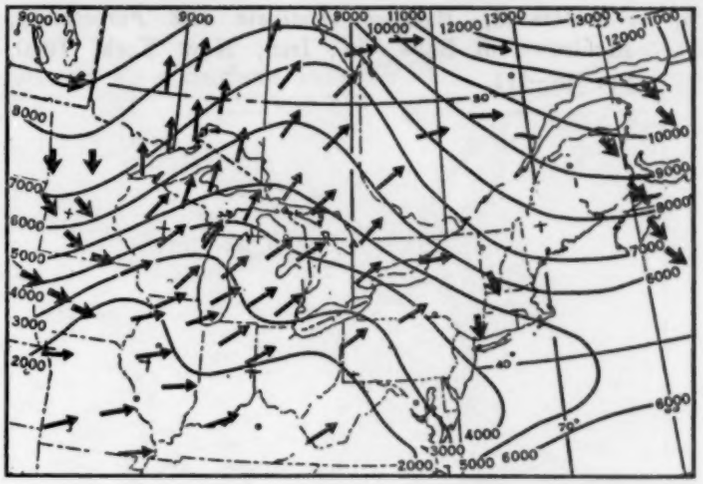

FIGURE 22.—229° A. isentropic chart for 1500 GMT, June 8, 1953.

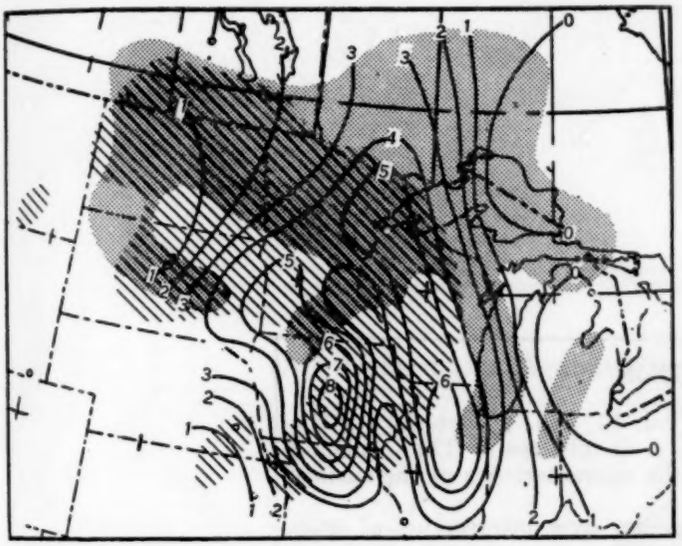

FIGURE 21.—Computed 12-hour lift in thousands of feet from 0300 GMT to 1500 GMT, June 8, 1953. The area where precipitation has occurred from 0330 GMT through 0930 GMT, June 8, is crosshatched, that from 1230 GMT through 1530 GMT, June 8, is shaded.

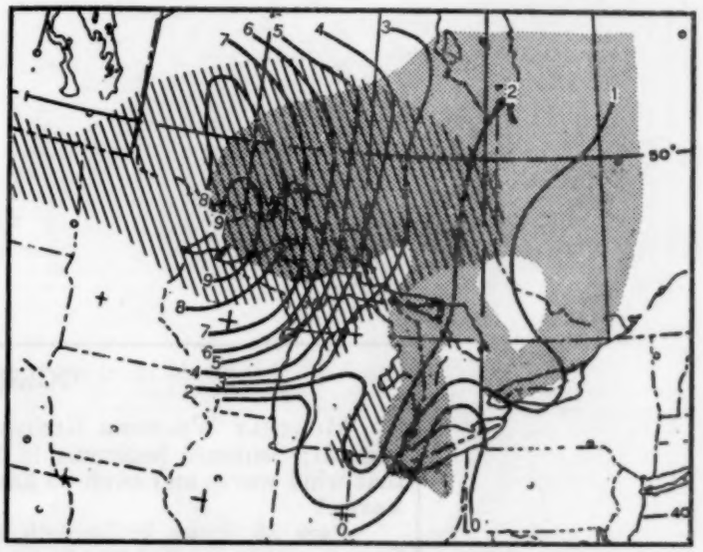

FIGURE 23.—Computed 12-hour lift from 1500 GMT, June 8, to 0300 GMT, June 9, 1953. The area where precipitation has occurred from 1530 GMT through 2130 GMT, June 8, is crosshatched, that from 0030 GMT, June 9, through 0330, GMT, June 9, is shaded.

CONCLUDING REMARKS

The main idea in this study of warm air advection has been to present a clear picture of the relationship between 1000-500-mb. thickness changes and sea level pressure changes. The method of computing vertical velocities, admittedly, is rough and extremely subjective, but it has the advantage of furnishing comparatively quick results.[1] Although the correlation between vertical motion and precipitation areas is favorable in this case, the notion needs considerable refinement. While this study has dealt primarily with warm air advection, many of the ideas employed are equally applicable to cold air advection.

[1] Some notable and more refined methods of computing vertical velocities have been developed by research units of the United States Air Force at New York University and by members of the New York University staff and the United States Weather Bureau. (For instance, see [6].)

REFERENCES

1. J. M. Austin, "Cloudiness and Precipitation in Relation to Frontal Lifting and Horizontal Convergence," 46 pp. (See pp. 15–16.) *Papers in Physical Oceanography and Meteorology*, vol. IX, No. 3, Massachusetts Institute of Technology and Woods Hole Oceanographic Institution, Cambridge and Woods Hole, Mass., 1943.
2. G. A. Lott, "An Extraordinary Rainfall Centered at Hallett, Okla.," *Monthly Weather Review*, vol. 81, No. 1, Jan. 1953, pp. 1–10.
3. H. R. Byers, *General Meteorology*, McGraw-Hill Book Co., Inc., New York, 1944, pp. 367–380, 211–214.
4. R. C. Bungaard, "A Procedure of Short-Range Weather Forecasting," *Compendium of Meteorology*, American Meteorological Society, Boston, 1952, pp. 766–795.

5. S. Petterssen, *Weather Analysis and Forecasting*, McGraw-Hill Book Co., Inc., New York, 1940, pp. 407–411.

6. J. E. Miller, et al, *A Study of Vertical Motion in the Atmosphere*, Dept. of Meteorology, New York University, N. Y., Feb. 1946, 68 pp.

CORRECTION

MONTHLY WEATHER REVIEW, vol. 81, No. 2, February 1953, page 37: Sentence beginning in line 1 should read "They indicate that wind waves and swell do have the characteristics of the surface waves."

Page 35, figure 3: Isopleth at center over intersection of cross lines should be labeled "8" instead of "9."

U. S. GOVERNMENT PRINTING OFFICE: 1953

Chart I. A. Average Temperature (°F.) at Surface, June 1953.

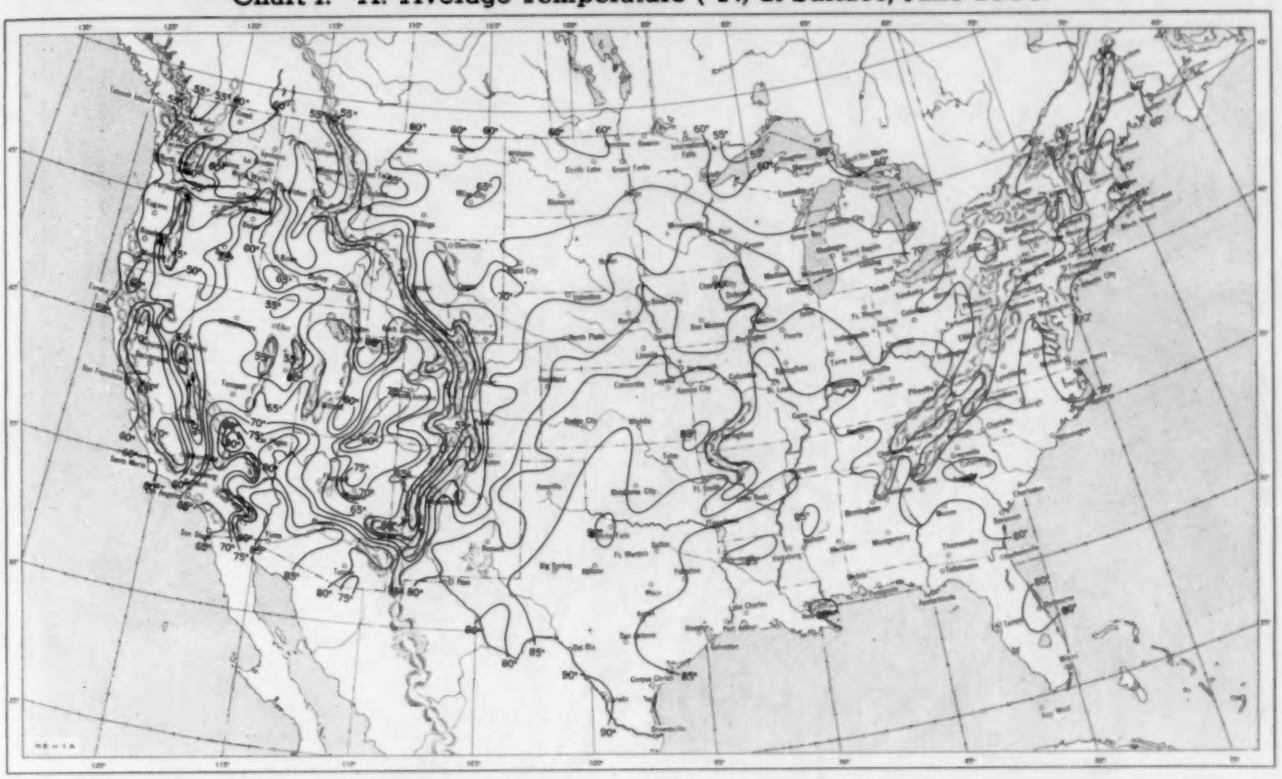

B. Departure of Average Temperature from Normal (°F.), June 1953.

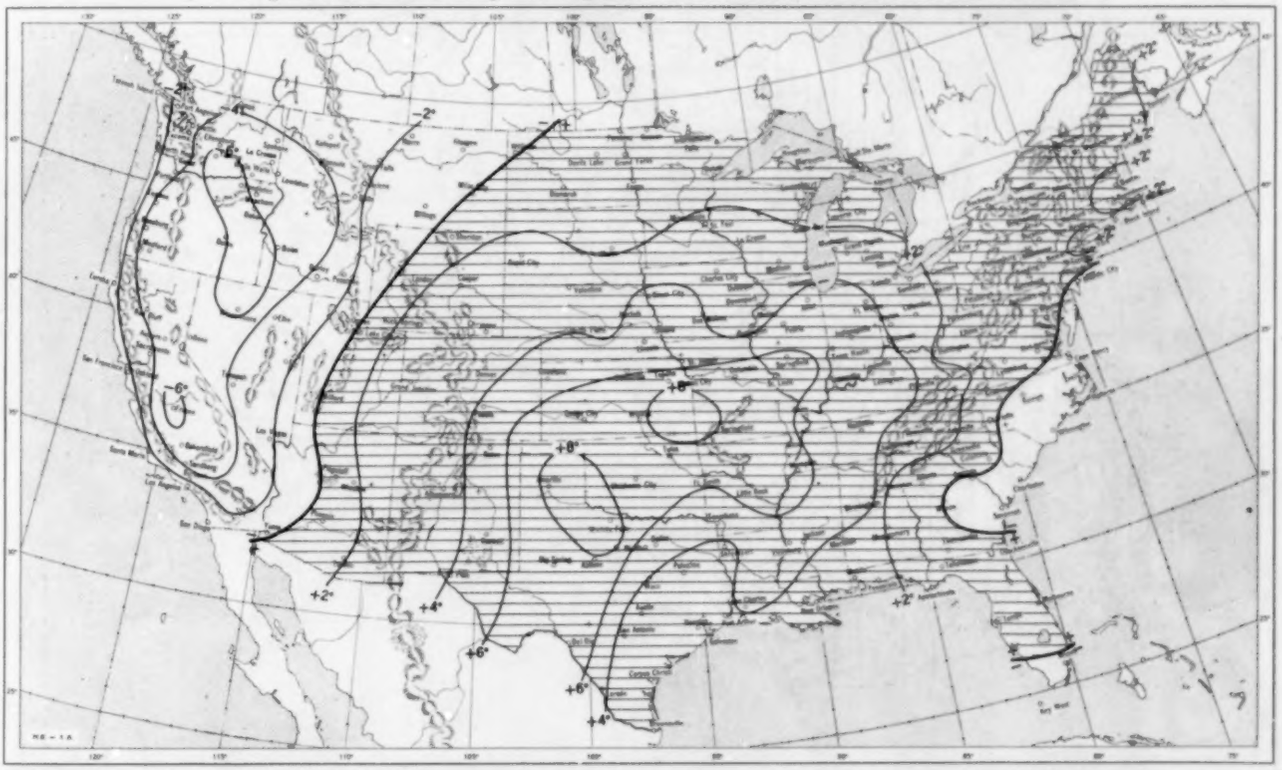

A. Based on reports from 800 Weather Bureau and cooperative stations. The monthly average is half the sum of the monthly average maximum and monthly average minimum, which are the average of the daily maxima and daily minima, respectively.
B. Normal average monthly temperatures are computed for Weather Bureau stations having at least 10 years of record.

Chart II. Total Precipitation (Inches), June 1953.

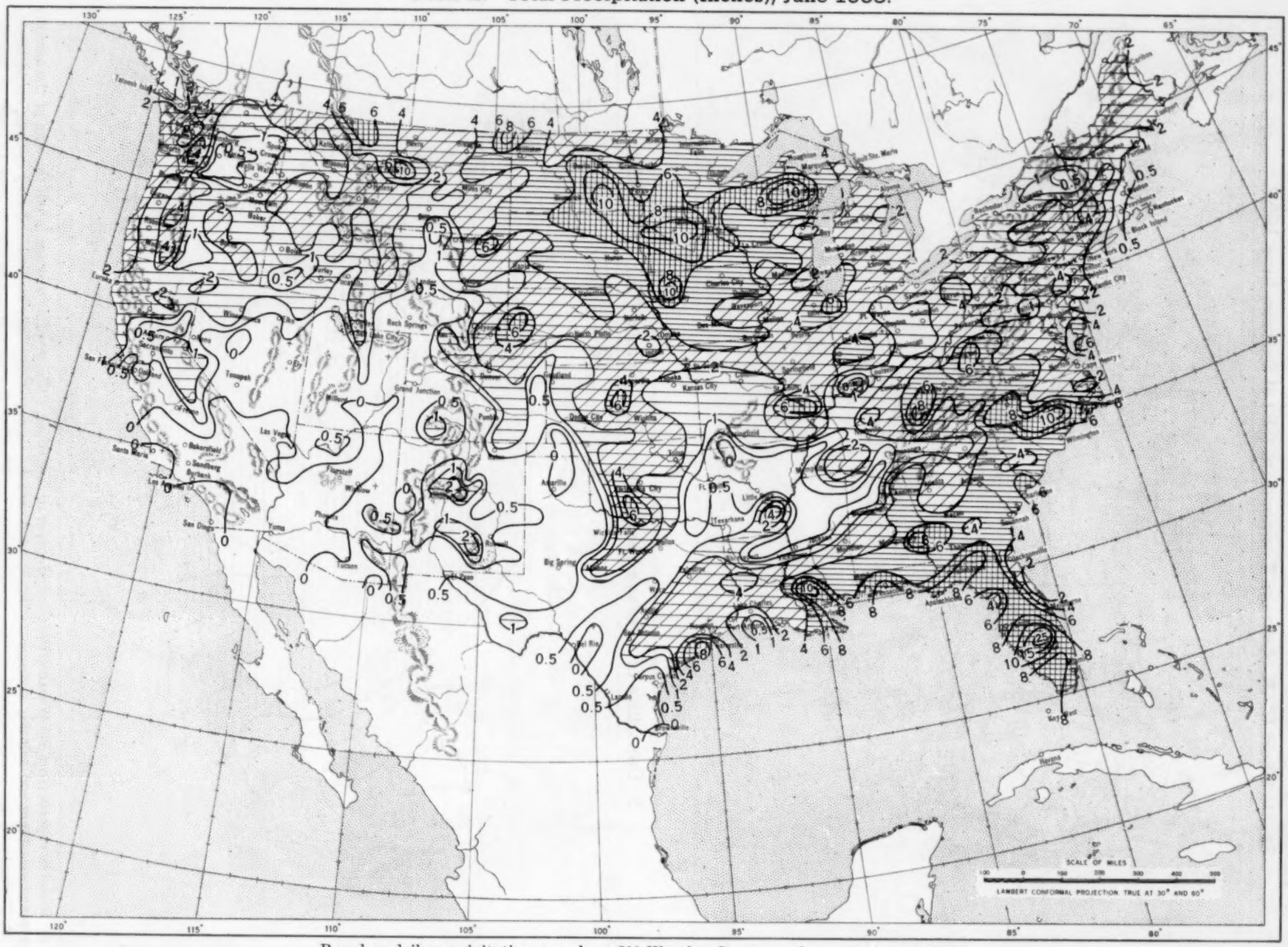

Based on daily precipitation records at 800 Weather Bureau and cooperative stations.

Chart III. A. Departure of Precipitation from Normal (Inches), June 1953.

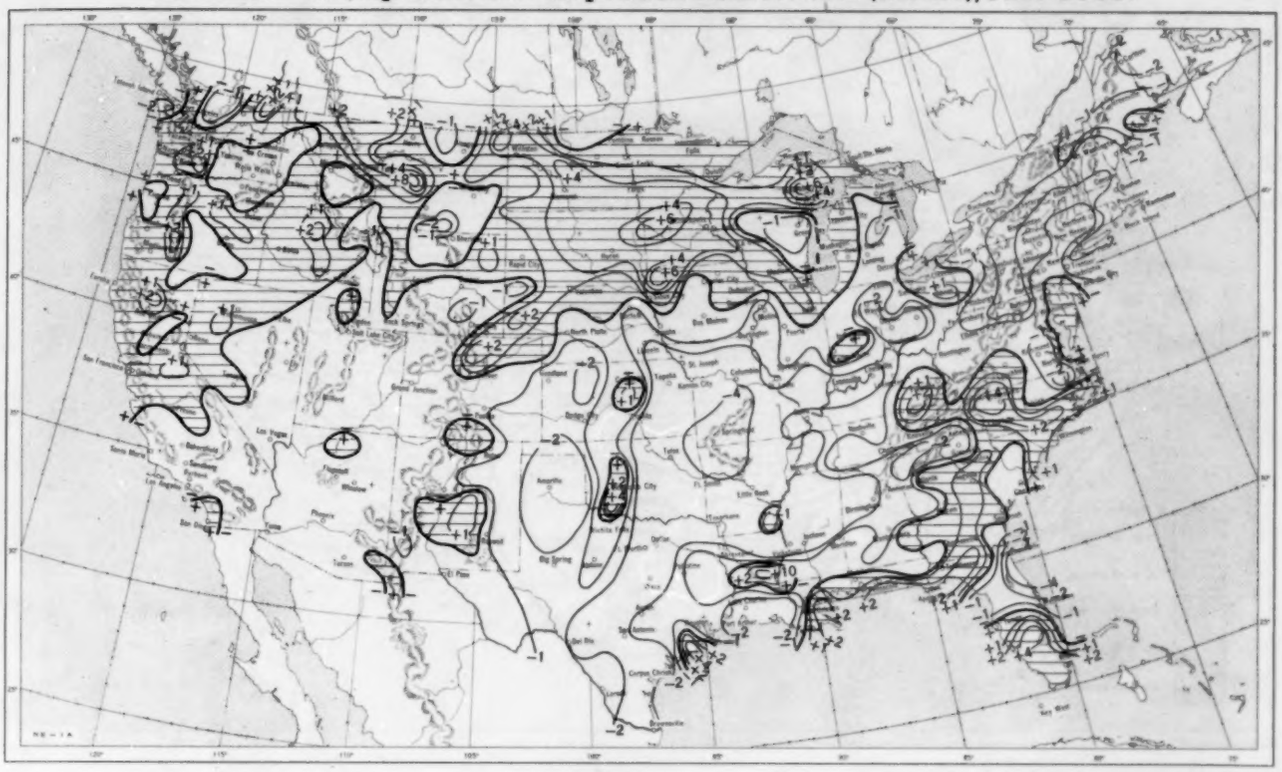

B. Percentage of Normal Precipitation, June 1953.

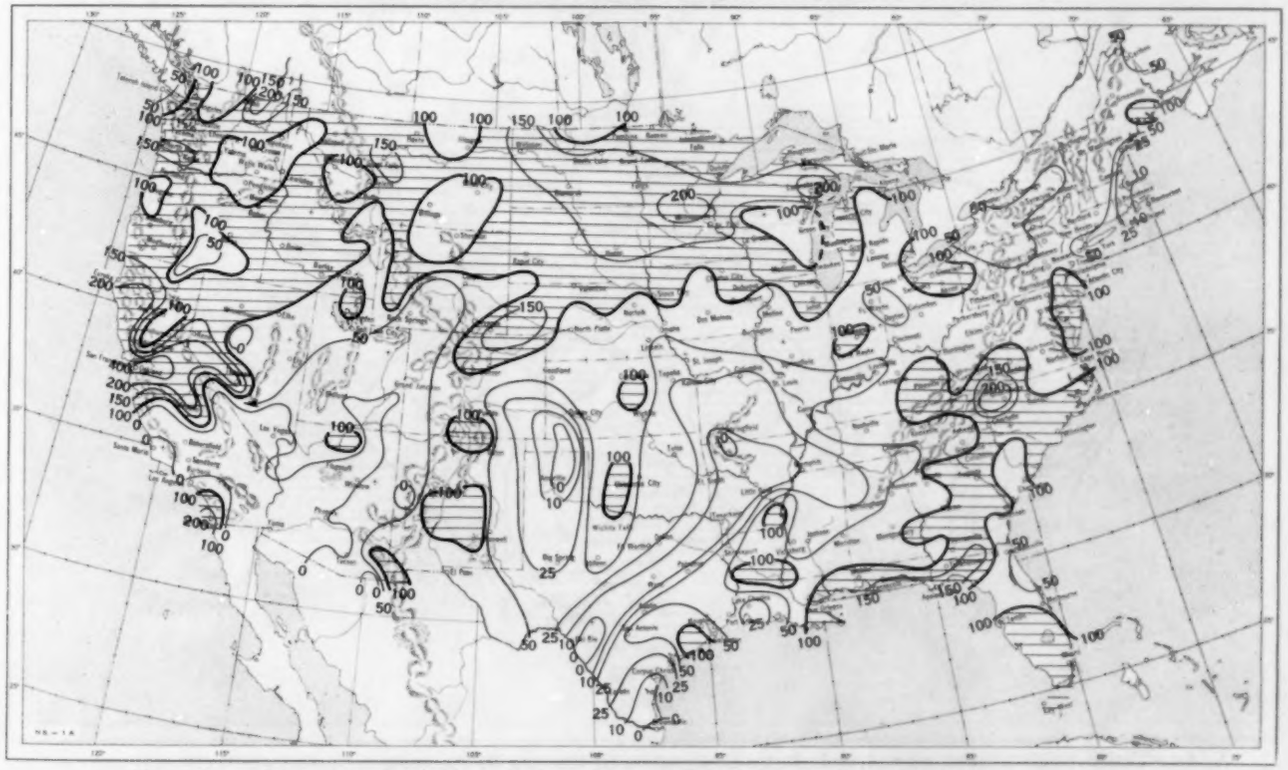

Normal monthly precipitation amounts are computed for stations having at least 10 years of record.

Chart VI. A. Percentage of Sky Cover Between Sunrise and Sunset, June 1953.

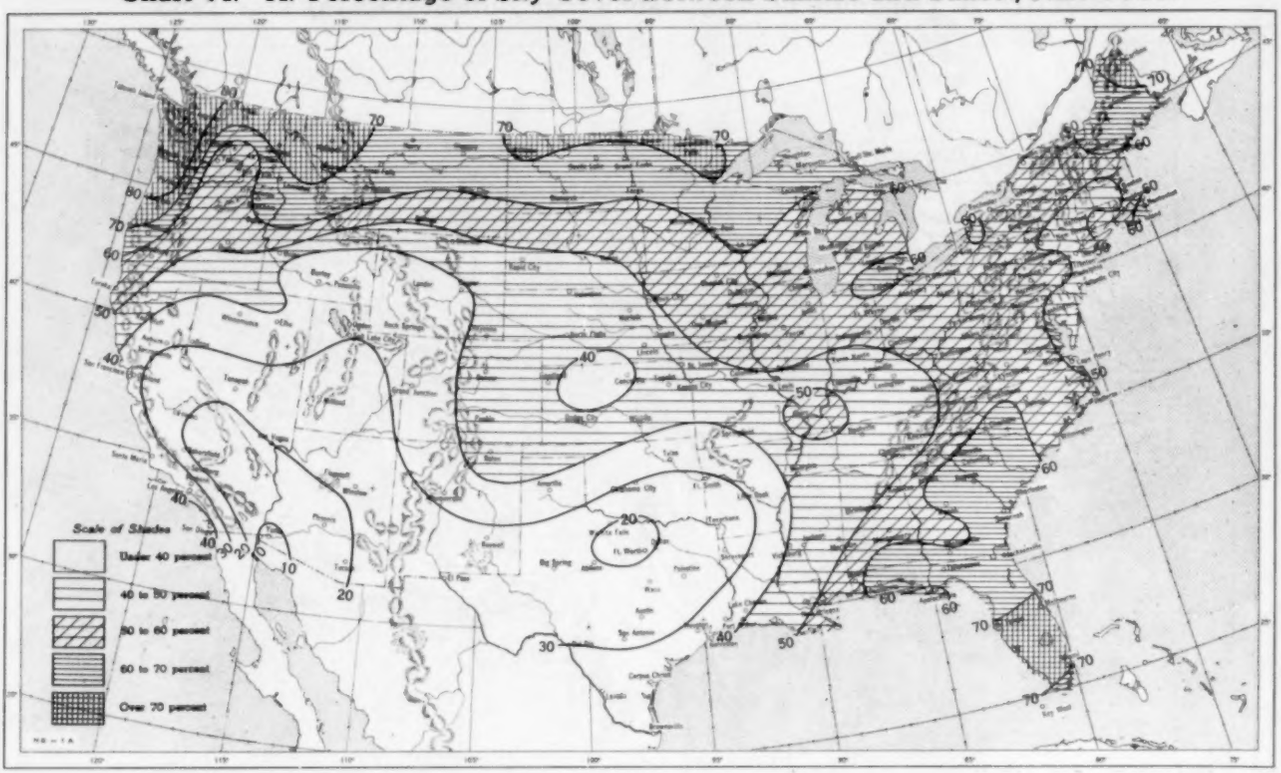

B. Percentage of Normal Sky Cover Between Sunrise and Sunset, June 1953.

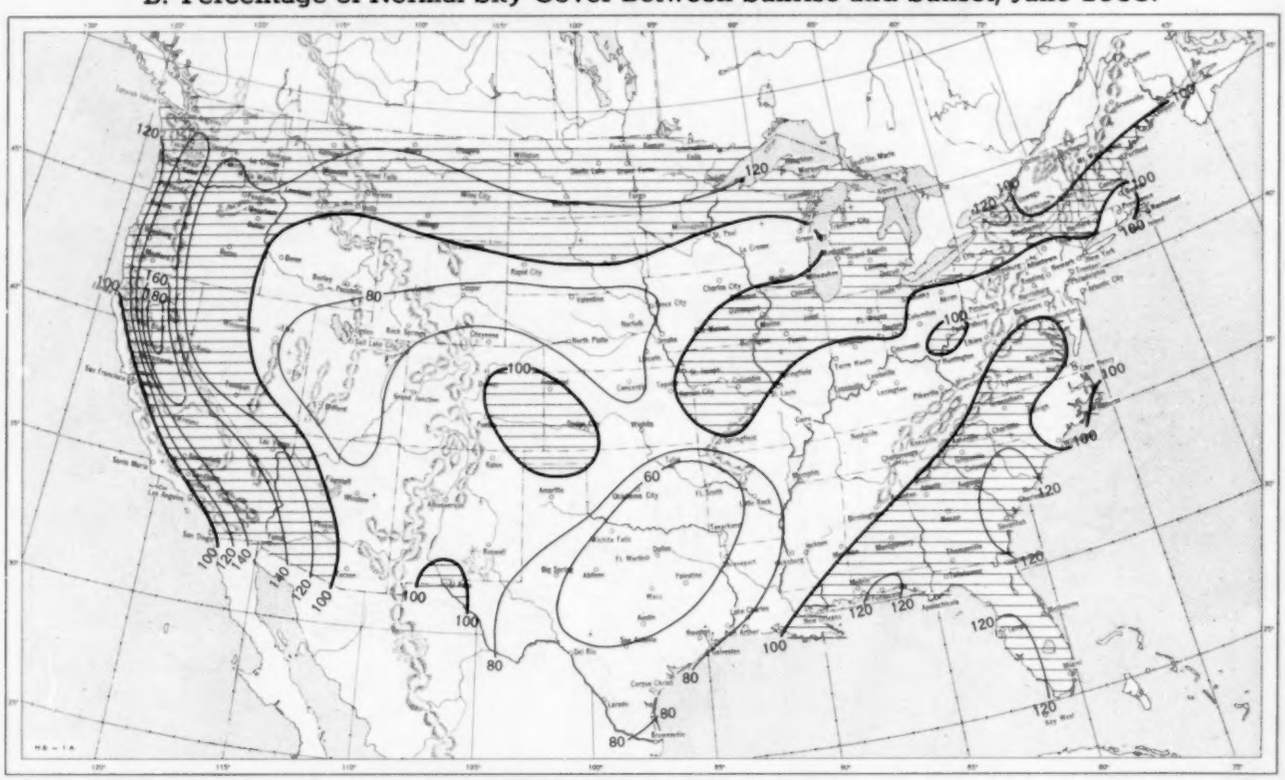

A. In addition to cloudiness, sky cover includes obscuration of the sky by fog, smoke, snow, etc. Chart based on visual observations made hourly at Weather Bureau stations and averaged over the month. B. Computations of normal amount of sky cover are made for stations having at least 10 years of record.

Chart VII. A. Percentage of Possible Sunshine, June 1953.

B. Percentage of Normal Sunshine, June 1953.

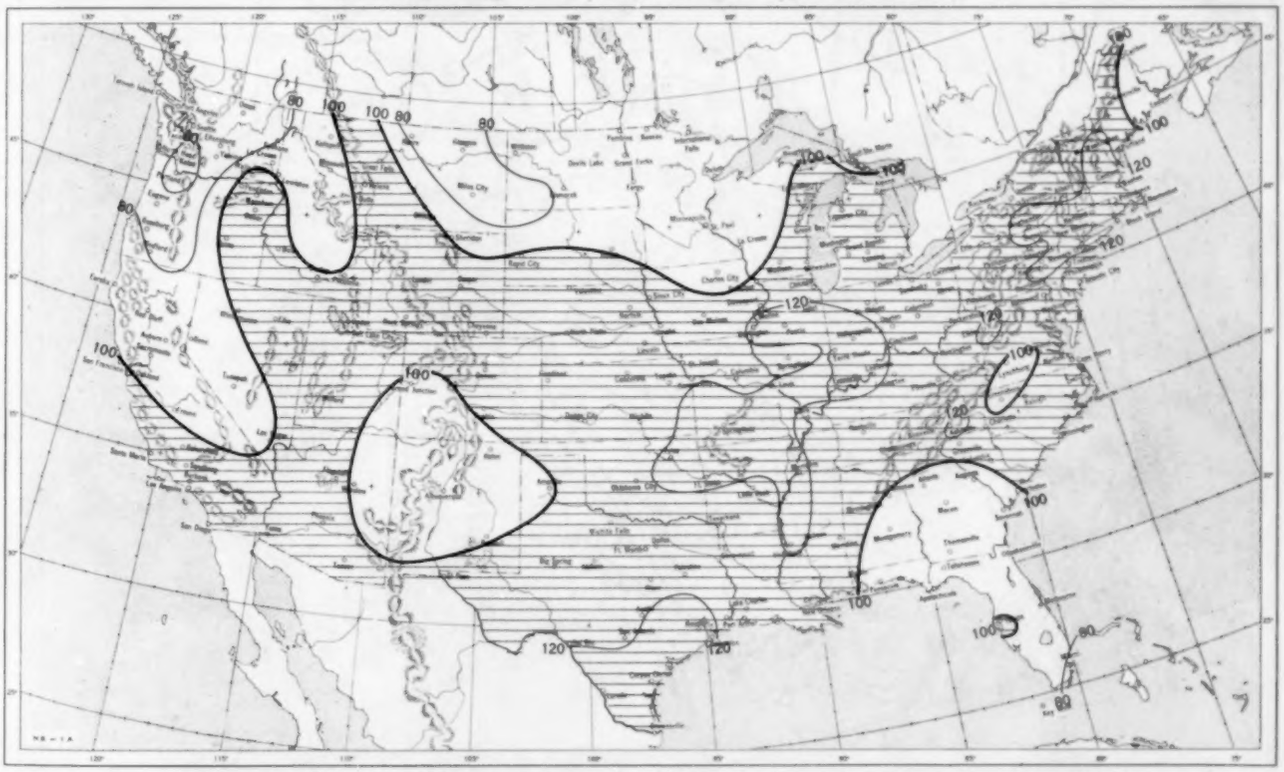

A. Computed from total number of hours of observed sunshine in relation to total number of possible hours of sunshine during month. B. Normals are computed for stations having at least 10 years of record.

Chart VIII. Average Daily Values of Solar Radiation, Direct + Diffuse, June 1953. Inset: Percentage of Normal Average Daily Solar Radiation, June 1953.

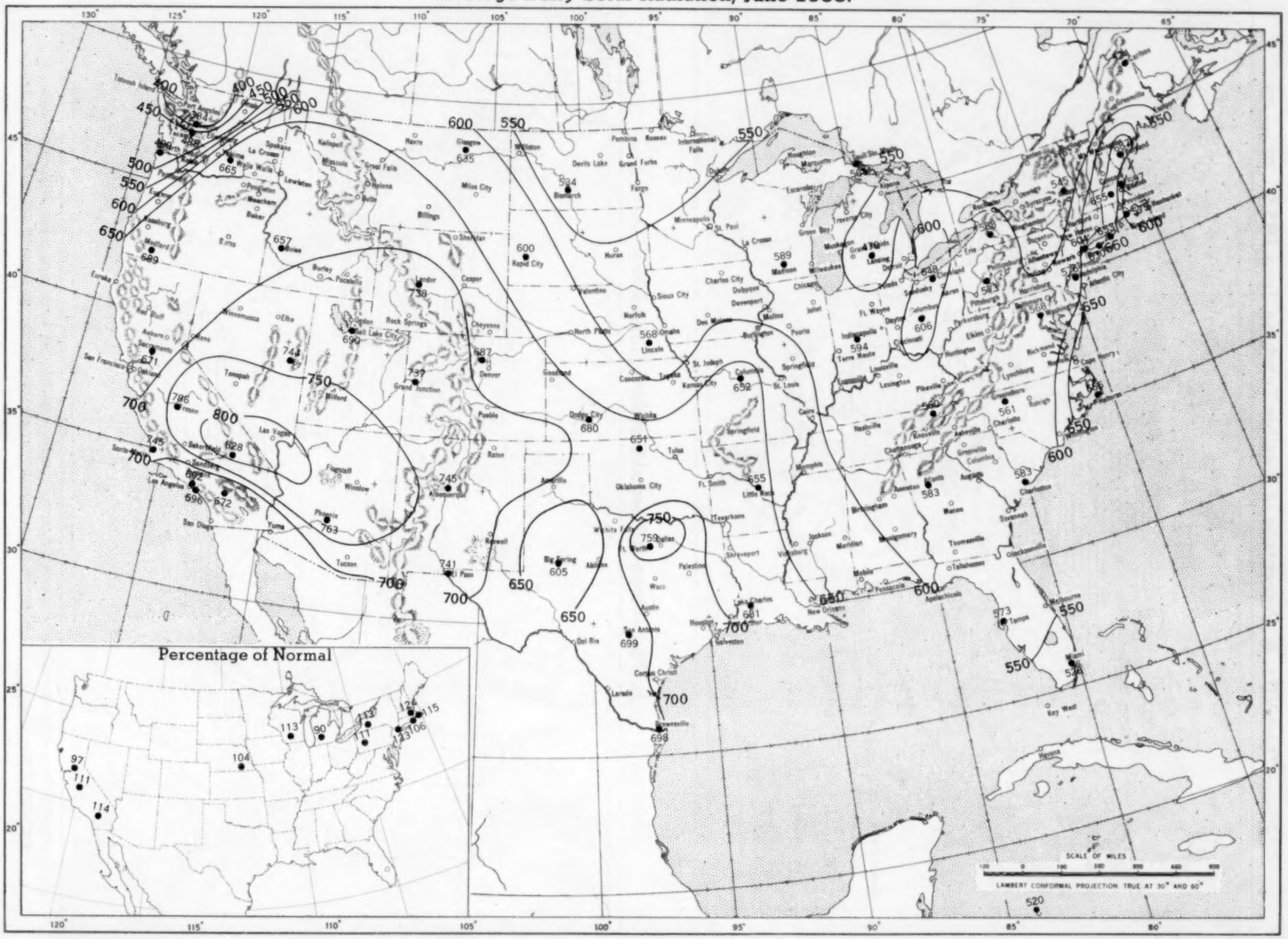

Chart shows mean daily solar radiation, direct + diffuse, received on a horizontal surface in langleys (1 langley = 1 gm. cal. cm. $^{-2}$). Basic data for isolines are shown on chart. Further estimates are obtained from supplementary data for which limits of accuracy are wider than for those data shown. Normals are computed for stations having at least 9 years of record.

are computed for stations having at least 9 years of record.

Chart IX. Tracks of Centers of Anticyclones at Sea Level, June 1953.

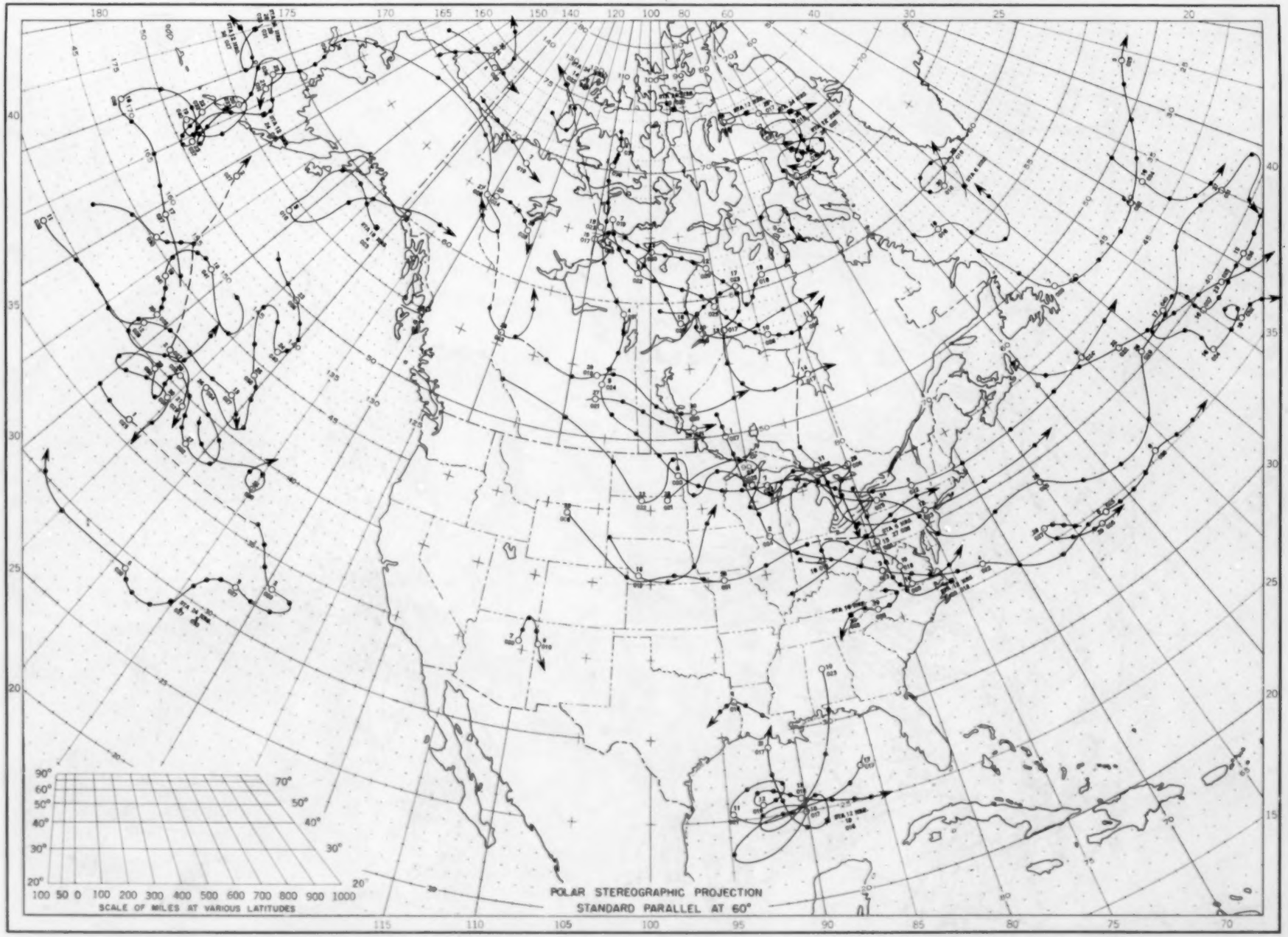

Circle indicates position of center at 7:30 a. m. E. S. T. Figure above circle indicates date, figure below, pressure to nearest millibar. Dots indicate intervening 6-hourly positions. Squares indicate position of stationary center for period shown. Dashed line in track indicates reformation at new position. Only those centers which could be identified for 24 hours or more are included.

Chart X. Tracks of Centers of Cyclones at Sea Level, June 1953.

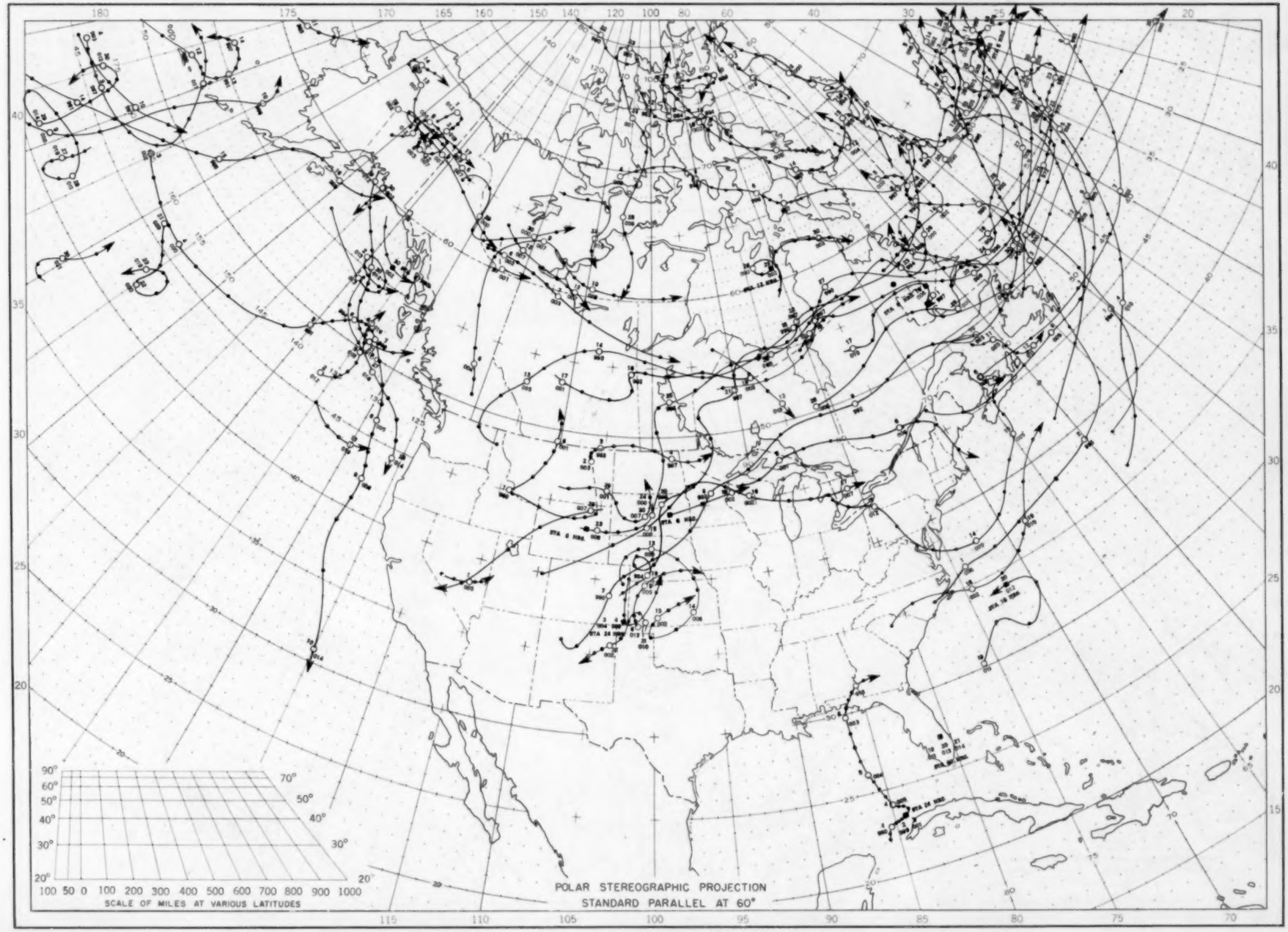

Circle indicates position of center at 7:30 a. m. E. S. T. See Chart IX for explanation of symbols.

Chart XI. Average Sea Level Pressure (mb.) and Surface Windroses, June 1953. Inset: Departure of Average Pressure (mb.) from Normal, June 1953.

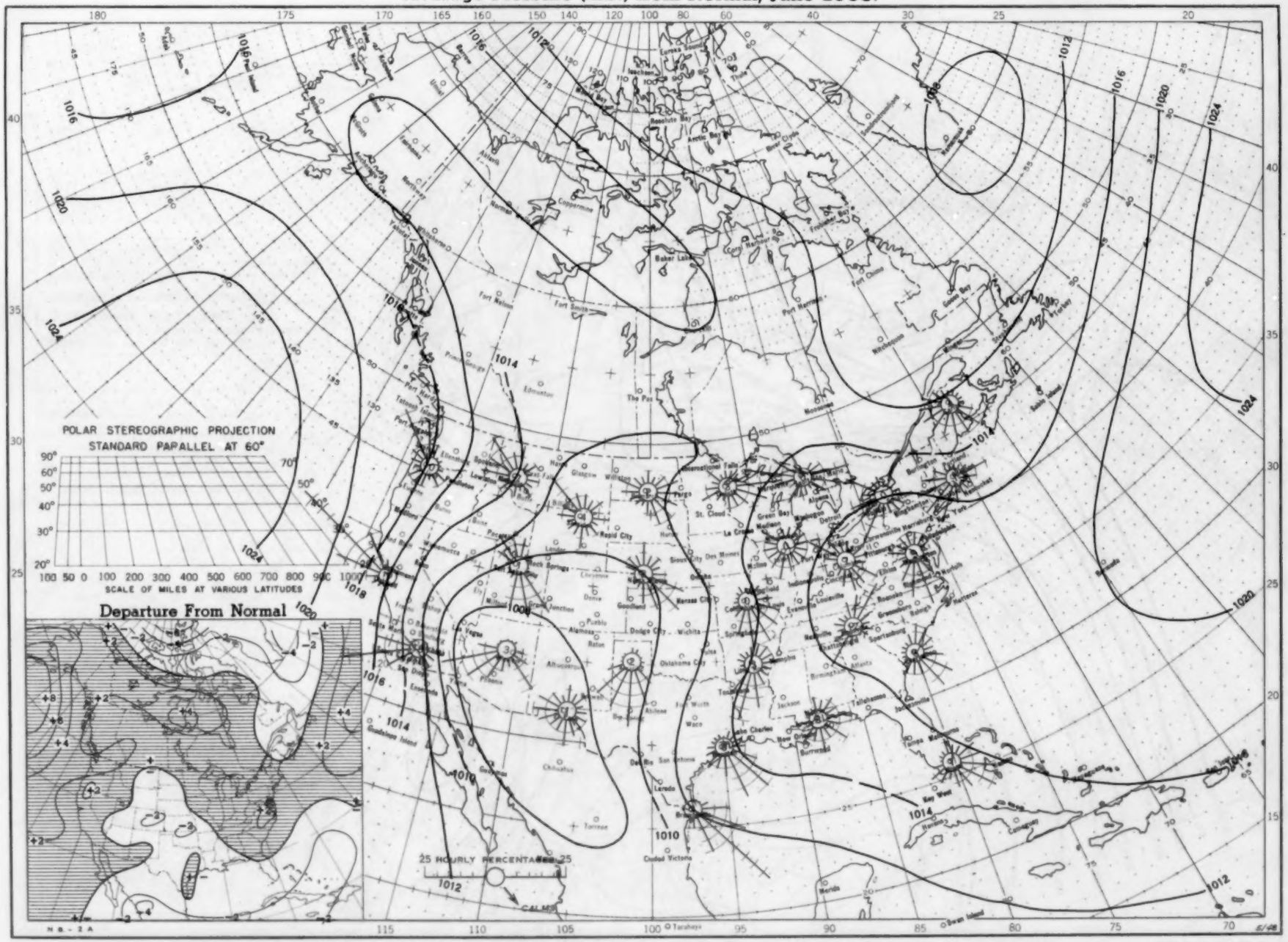

Average sea level pressures are obtained from the averages of the 7:30 a. m. and 7:30 p. m. E. S. T. readings. Windroses show percentage of time wind blew from 16 compass points or was calm during the month. Pressure normals are computed for stations having at least 10 years of record and for 10° intersections in a diamond grid based on readings from the Historical Weather Maps (1899-1939) for the 20 years of most complete data coverage prior to 1940.

Chart XII. Average Dynamic Height in Geopotential Meters (1 g.p.m. = 0.98 dynamic meters) of the 850-mb. Pressure Surface, Average Temperature in °C. at 850 mb., and Resultant Winds at 1500 Meters (m.s.l.), June 1953.

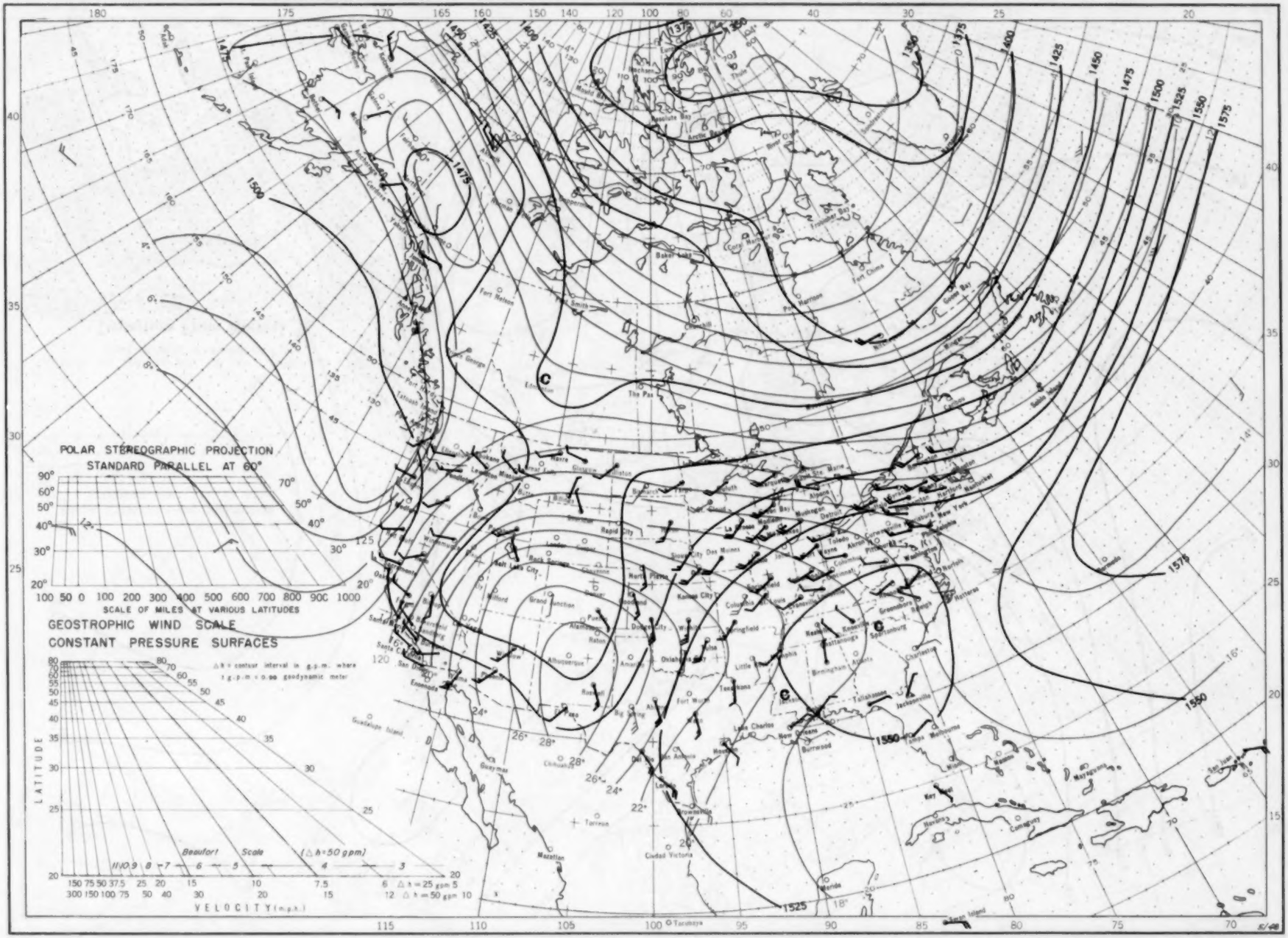

Contour lines and isotherms based on radiosonde observations at 0300 G. M. T. Winds shown in black are based on pilot balloon observations at 2100 G. M. T.; those shown in red are based on rawins taken at 0300 G. M. T.

Chart XIII. Average Dynamic Height in Geopotential Meters (1 g.p.m.. = 0.98 dynamic meters) of the 700-mb. Pressure Surface, Average Temperature in °C. at 700 mb., and Resultant Winds at 3000 Meters (m.s.l.), June 1953.

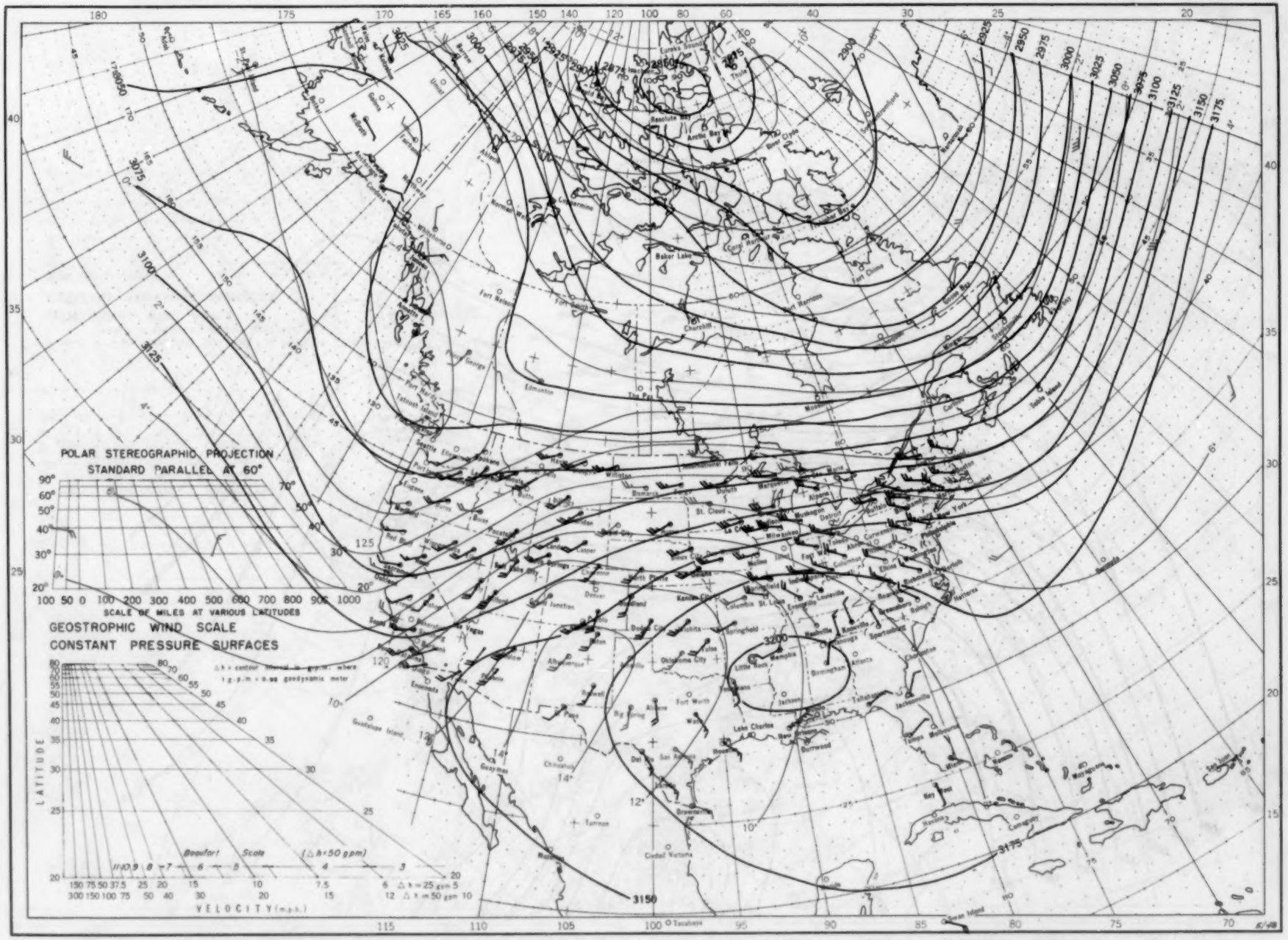

Contour lines and isotherms based on radiosonde observations at 0300 G. M. T. Winds shown in black are based on pilot balloon observations at 2100 G. M. T.; those shown in red are based on rawins taken at 0300 G. M. T.

Chart XIV. Average Dynamic Height in Geopotential Meters (1 g.p.m. = 0.98 dynamic meters) of the 500-mb. Pressure Surface, Average Temperature in °C. at 500 mb., and Resultant Winds at 5000 Meters (m.s.l.), June 1953.

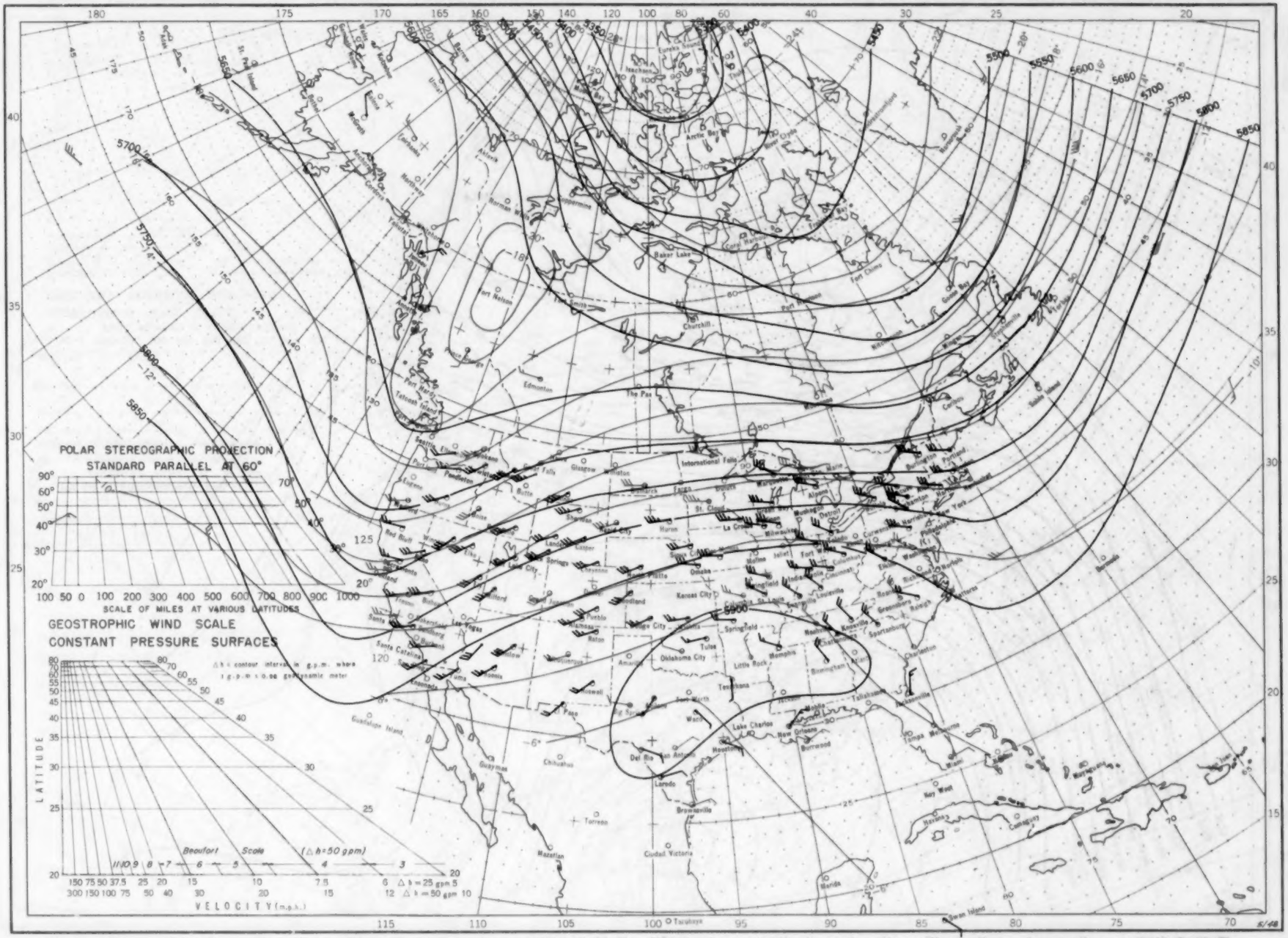

Contour lines and isotherms based on radiosonde observations at 0300 G. M. T. Winds shown in black are based on pilot balloon observations at 2100 G. M. T.; those shown in red are based on rawins at 0300 G. M. T.

Chart XV. Average Dynamic Height in Geopotential Meters (1 g.p.m. = 0.98 dynamic meters) of the 300-mb. Pressure Surface, Average Temperature in °C. at 300 mb., and Resultant Winds at 10,000 Meters (m.s.l.), June 1953.

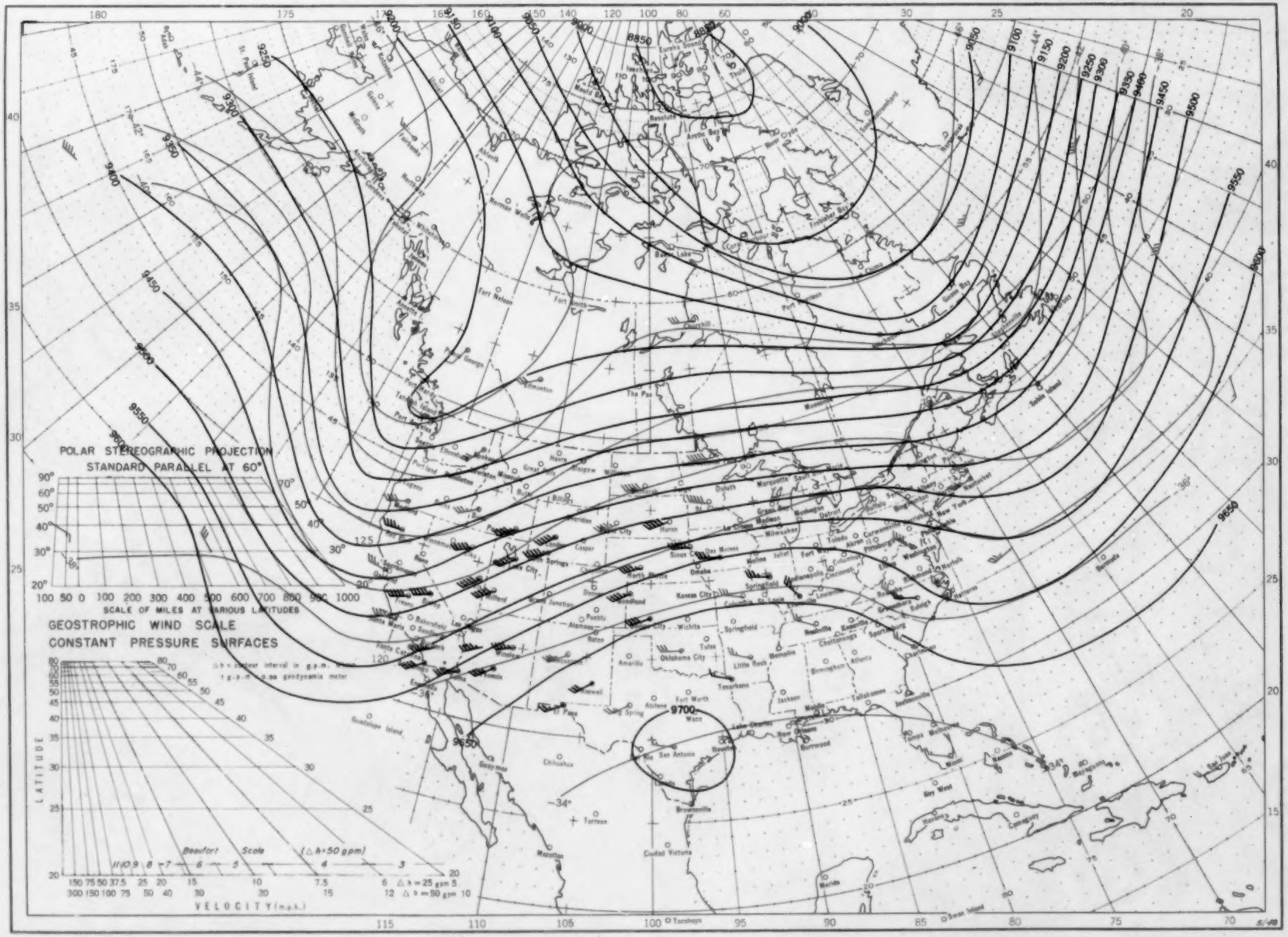

Contour lines and isotherms based on radiosonde observations at 0300 G. M. T. Winds shown in black are based on pilot balloon observations at 2100 G. M. T.; those shown in red are based on rawins at 0300 G. M. T.